CHAPTER 49 ■ GENITAL TRACT—CT, MR, AND RADIOGRAPHIC IMAGING

WILLIAM E. BRANT

FEMALE GENITAL TRACT

The primary modality for imaging of the female genital tract is US using transabdominal, transvaginal, and Doppler techniques. Sonography of the genital tract is reviewed in Chapter 51. MR and CT are used to stage and follow-up pelvic malignancies and to supplement US by providing additional characterization of lesions. MR, because of its excellent capacity to differentiate tissue types, is particularly useful in making an imaging diagnosis of pelvic disease. Diffusion-weighted MR has potential to aid in the discrimination between benign and malignant lesions and to provide improved detection of peritoneal metastases and tumor recurrence. MDCT with isotropic voxel acquisition allows for multiplanar reformatted images of high quality to improve recognition of anatomic variants and complex pathology. In addition, many uterine and adnexal lesions may be discovered incidentally by pelvic CT or MR performed for other reasons. Hysterosalpingography (HSG) is combined with US, CT, and MR to diagnose congenital anomalies of the female genital tract and mechanical causes of infertility. The HSG is performed by cannulating the cervix and injecting a contrast agent into the cavity of the uterus and fallopian tubes. Free communication of these lumina with the peritoneal cavity is evidenced by free spill of the contrast agent into the peritoneal cavity outlining loops of bowel. Sonohysterography is an alternative to HSG. Isotonic saline is injected into the uterine cavity while the uterus is examined sonographically. Virtual HSG is an emerging MDCT technique that offers the potential of high-resolution images depicting both the internal and external surfaces of the uterus and fallopian tubes.

Anatomy

The uterus is a pear-shaped muscular organ located between the bladder and rectum. The anterior and posterior surfaces of the uterus are covered by peritoneum, the folds of which extend laterally to the pelvic sidewalls forming the *broad ligament*. Peritoneum reflecting off the uterus and the bladder forms a shallow anterior vesicouterine pouch. A "bare area" of extraperitoneal space is present between the lower uterus and bladder. This is an important area for direct spread of tumor from one organ to the other. Posteriorly the peritoneum reflects onto the rectum and forms a deep recto-uterine pouch or cul-de-sac. The peritoneum completely covers the uterus and the posterior vaginal fornix. Only the thin wall of the vagina separates the vaginal cavity from the cul-de-sac, allowing transvaginal access to the intraperitoneal space for US-guided culdocentesis or biopsy. The uterus, cervix, and upper one-third of the vagina are derived from the Müllerian ducts, while the lower two-thirds of the vagina arise from the urogenital sinus. *Parametrium* refers to the connective tissue adjacent to the uterus between the folds of the broad ligament and adjacent to the vagina. Uterine vessels and lymphatics pass through the parametrium. The broad ligament covers the fallopian tubes hanging over them like a sheet folded on a clothesline enveloping the vessels of the parametrium. The broad ligament is well outlined when fluid is present in the pelvic peritoneal cavity. The fundus of the uterus is that portion that extends cephalad from the origin of the fallopian tubes. The body extends from the fallopian tubes to the isthmus, a slight constriction that marks the location of the internal cervical os. The cervix is cylindrical in shape and 3 to 4 cm in length. Its lower portion, including the external os, protrudes into the vagina and is surrounded by the vaginal fornices. The ureters pass 2 cm lateral to the supravaginal portion of the cervix. The ***vagina*** is a muscular tube that is a flattened oval shape on cross-sectional images. The urethra is a prominent tubular structure that courses in the anterior wall of the vagina.

Ovaries vary in size and appearance depending on the woman's age, hormonal status, and stage of the menstrual cycle. The adult ovary is oval with maximal dimensions of 5 × 3 × 2 cm. Abnormalities of size are best determined by calculating ovarian volume using the formula (length × width × thickness × 0.52). Maximum ovarian volume is 9 cc before menarche, 22 cc in menstruating women, and 6 cc in postmenopausal women. The location of the ovaries is variable in different patients and even in the same patient at different times depending on degree of bladder filling and the presence and size of other structures in the pelvis. The typical location is lateral, superior, or posterior to the uterine fundus, or in the cul-de-sac. When the uterus is retroverted the ovaries are anterior or lateral to the uterus. The pelvic ureters form an important anatomic landmark that assist in the recognition of the origin of pelvic masses. The ovaries are anterior to the ureters, so an ovarian mass will displace the ureter posteriorly or

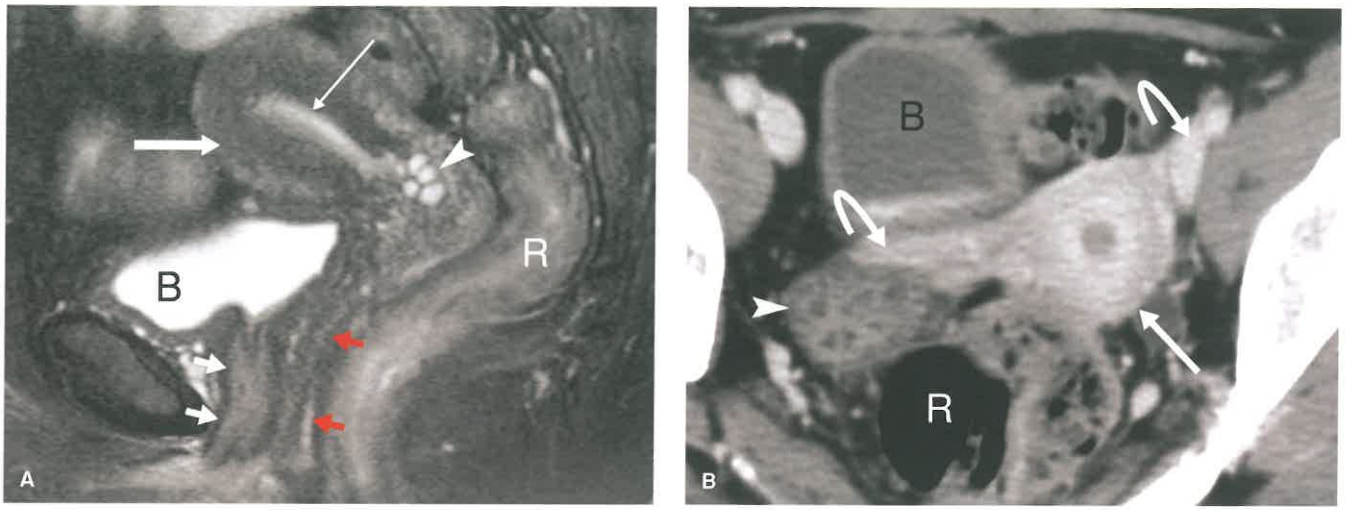

FIGURE 49.1. **Normal Uterus. A:** Sagittal T2-weighted MR image shows the uterus (*large arrow*), and the high signal intensity endometrium (*skinny arrow*) surrounded by the low signal intensity junctional zone myometrium. Multiple nabothian cysts (*arrowhead*) are present in the endocervical canal. The vagina (*short red arrows*) is shown as a low signal intensity muscular tube with the urethra (*short white arrows*) coursing in its anterior wall. High signal urine identifies the bladder (*B*) anteriorly. The rectum (*R*) is seen posteriorly. **B:** Axial postcontrast CT image shows the uterus (*arrow*) in transverse plane with enhancing endometrium surrounding a small volume of low attenuation fluid in the uterine cavity. The broad ligaments (*curved arrows*) enveloping the enhancing fallopian tubes and parametrial vessels extend laterally from the uterus to the right ovary (*arrowhead*). The bladder (*B*) containing low attenuation urine without contrast creates a fluid layer with high attenuation urine containing excreted contrast. The rectum (*R*) containing gas is seen posteriorly.

posterolaterally. Iliac lymph nodes are lateral to ureters, so adenopathy will displace the ureters medially or anteromedially.

Normal MR Anatomy. The internal anatomy of the uterus is depicted best on T2WI. On T2WI, the *endometrium* appears as a high signal intensity central stripe surrounded by the low signal intensity *junctional zone* myometrium (Fig. 49.1). The endometrium may normally be up to 14 mm in thickness in women of menstrual age. The bulk of the *myometrium* is intermediate signal intensity. The low signal intensity of inner junctional zone of the myometrium on T2WI is due to lower water content. On T1WI, the entire uterus is low in signal intensity and the internal anatomy of the uterus is poorly demonstrated. With gadolinium enhancement, uterine zonal anatomy becomes evident on T1WI. The cervix is largely composed of collagenous tissues that are low in signal intensity on both T1WI and T2WI, providing a dark background for visualization of hyperintense cervical carcinomas. The endocervical epithelium and mucus are homogeneous high signal on T2WI. High-resolution MR using surface or intravaginal coils shows two zones in the cervical fibromuscular stroma, a darker inner zone contiguous with the uterine junctional zone and an intermediate signal outer zone distinctly darker than the myometrium. Vaginal anatomy is also best seen on T2WI, which shows the muscular vaginal wall as low in signal with the epithelium and mucus as high in signal. Aqueous vaginal gel may be inserted for MR scanning to distend the vagina and optimize evaluation of the vagina and cervix. The normal ovaries of fertile women are easily identified by the bright signal of the follicles on T2WI (Fig. 49.2). The follicles are low or intermediate in signal on T1WI. The cortex of the ovary in the premenopausal woman is darker in the signal than the medulla on T2WI. The postmenopausal ovary is more difficult to identify because of the absence of follicles and the cortex and medulla being nearly equal in signal on both T1WI and T2WI.

MR is sensitive to physiologic changes that affect the uterus and ovary during the menstrual cycle. Signal intensity of the myometrium is highest during late proliferative and early secretory phases and is lowest during menstruation and early proliferative phase. Low-intensity myometrial lesions such as leiomyomas and adenomyomas are best demonstrated when the myometrium has the highest signal intensity in midmenstrual cycle. The ovaries vary in size and appearance during the menstrual cycle and are largest with a dominant follicle just prior to ovulation.

Normal CT Anatomy. Because the position of the uterus is so variable on axial plane CT the outline of the uterus often appears lobulated or bulbous solely because of position (Fig. 49.1). The uterus is uniform in soft tissue attenuation and its internal anatomy is not well demonstrated by unenhanced CT. Because the myometrium is highly vascular, the uterus enhances more than most other pelvic organs. Fluid in the uterine cavity is usually low density. The ovaries are easily mistaken for unopacified bowel loops in the pelvis. Ovarian follicles are recognized by their fluid attenuation (Fig. 49.2). The vagina is seen in cross-section as a flattened ellipse of soft tissue density between the bladder and rectum. Normal fallopian tubes are usually not evident on CT. Multiplanar reformatted MDCT images are of great value in interpretation of complex pelvic anatomy and pathology.

Hysterosalpingography is primarily used for the evaluation of infertility to demonstrate the morphology and patency of the uterine canal and fallopian tubes (Fig. 49.3). Contrast injected into the uterine cavity outlines the endocervical canal, uterine cavity, and lumen of the fallopian tubes with free spill of contrast into the peritoneal cavity in the normal patient. The uterine cavity is sharply defined and triangular in shape with normal mild concavity in the fundal region. The size of the cavity varies with parity. The endocervical canal is cylindrical in shape, 3 to 4 cm in length, and 1 to 3 cm in width. Folds in the endocervical mucosa form a normal serrated appearance. The normal fallopian tubes are 10 to 12 cm in length extending from the cornua of the uterus. The lumen is thread-like (1 to 2 mm) until it reaches the ampulla where it expands to 5 to 10 mm and rugal folds become visible. Patency of the tubes is confirmed by dispersal of contrast within the peritoneal cavity outlining loops of bowel.

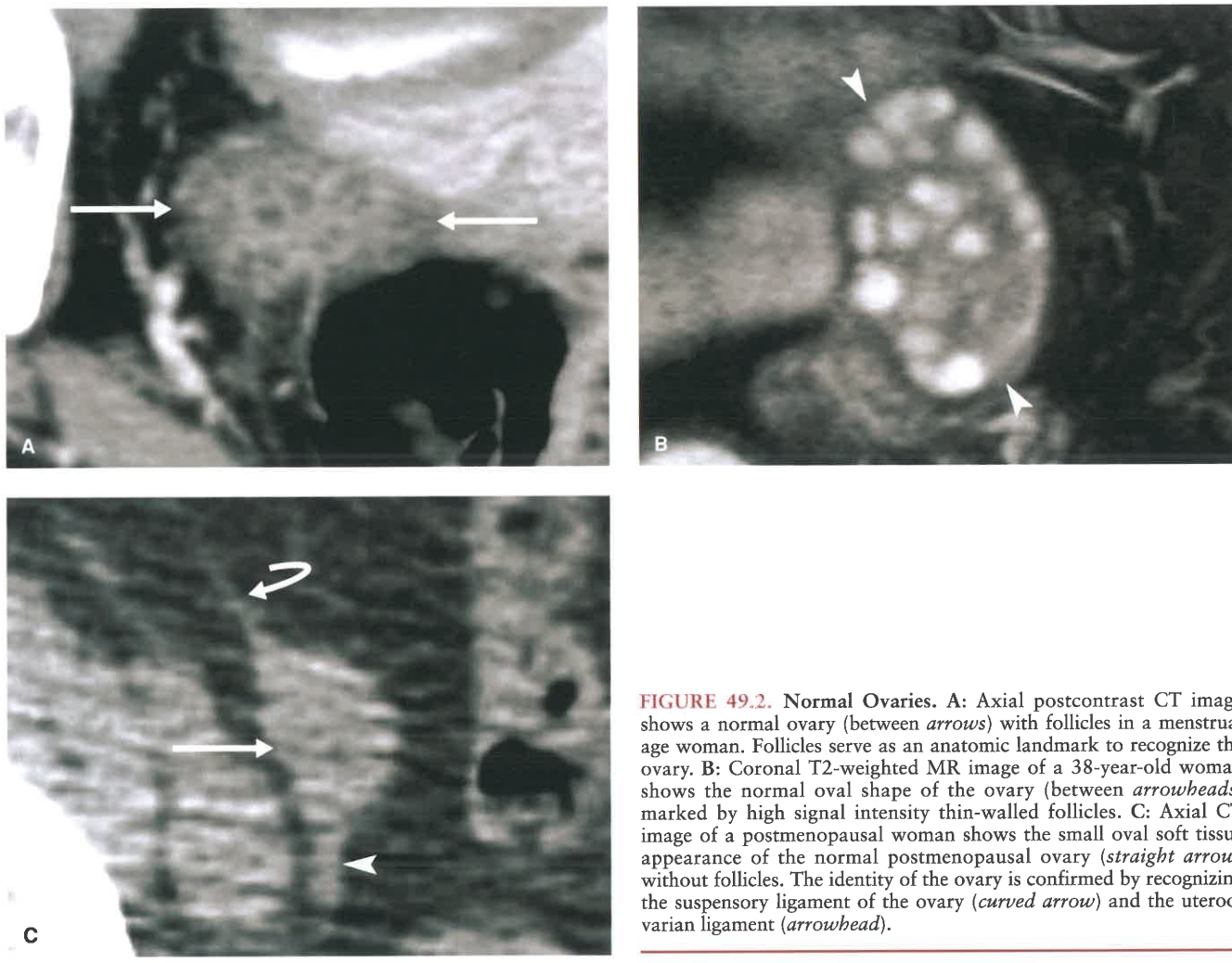

FIGURE 49.2. **Normal Ovaries. A:** Axial postcontrast CT image shows a normal ovary (between *arrows*) with follicles in a menstrual age woman. Follicles serve as an anatomic landmark to recognize the ovary. **B:** Coronal T2-weighted MR image of a 38-year-old woman shows the normal oval shape of the ovary (between *arrowheads*) marked by high signal intensity thin-walled follicles. **C:** Axial CT image of a postmenopausal woman shows the small oval soft tissue appearance of the normal postmenopausal ovary (*straight arrow*) without follicles. The identity of the ovary is confirmed by recognizing the suspensory ligament of the ovary (*curved arrow*) and the uteroovarian ligament (*arrowhead*).

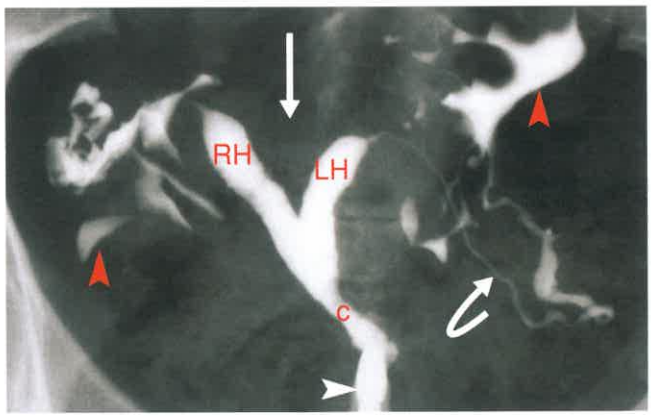

FIGURE 49.3. **Septate Uterus.** HSG demonstrates two horns of the uterine cavity (*RH, LH*) separated by a muscular septum (*arrow*). The delicate lumen of the left fallopian tube is well demonstrated (*curved arrow*), while the lumen of the right fallopian tube is obscured by the superimposed contrast. Free spill of contrast into the peritoneal cavity is evident (*red arrowheads*), confirming the patency of the fallopian tubes. Iodinated contrast agent was injected into the uterus after placing a cannula (*white arrowhead*) into the cervix (*c*).

Congenital Anomalies

Congenital anomalies of the female genital tract are a common cause of infertility, seen in up to 9% of women evaluated for infertility or repeated spontaneous abortion. In addition, unrecognized anomalies may be mistaken for other types of pathology, such as leiomyoma. Most anomalies result from arrested development or incomplete fusion of the paired Müllerian duct that forms the uterus, cervix, and fallopian tubes. Urinary tract abnormalities are found in 20% to 50% of patients with uterine anomalies. Arrested Müllerian duct development may result in uterine aplasia or unicornuate uterus with a single fallopian tube. Ipsilateral renal agenesis is found in 5% to 20% of patients with these anomalies. Failure of complete fusion of the Müllerian duct results in varying degrees of duplication, from *uterus didelphys*, with two uteri, two cervices, and two vaginas; to *bicornuate uterus* with two uterine horns, one (*unicollis*) or two (*bicollis*) cervices, and one vagina; to an *arcuate* (septate) uterus with a midline septum dividing the uterus into two cavities (Figs. 49.3 and 49.4). Uterine anomalies should be suspected when the uterus appears abnormal in size, contour, or position. The classification of the anomaly is made by a combination of physical examination and MR examination. HSG is used to demonstrate the uterine cavity and fallopian tubes.

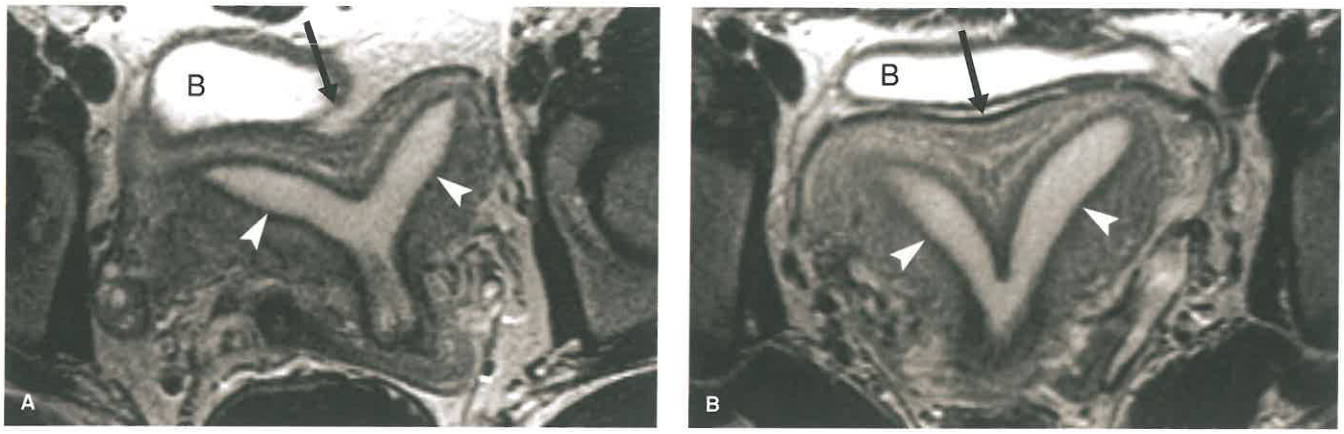

FIGURE 49.4. **Uterine Anomalies. A:** Bicornuate uterus. **B:** Septate uterus. T2-weighted axial images of the uterus in two patients demonstrate the characteristic difference between a bicornuate uterus, (**A**), with a surface indentation at the fundus (*arrow*) dividing the uterus into two separate horns (*arrowheads*) and a septate uterus, (**B**), showing a thick muscular septum and only a slight surface indentation at the fundus (*arrow*). Two uterine cavities (*arrowheads*) are present in both cases. Uterine anomalies represent a continuous spectrum of abnormality. *B*, bladder.

Benign Conditions

Leiomyomas are the most common uterine tumor affecting 50% of women of reproductive age. Most women are asymptomatic but the tumors may cause excessive bleeding, pelvic pain, mass symptoms, and infertility. Tumors are benign and made up of smooth muscle and a variable amount of fibrous tissue. Tumors with scant fibrous tissue enhance brightly while those with abundant fibrous tissue enhance poorly. Most tumors are intramural (within the myometrial wall), while others are submucosal (beneath the endometrium) or subserosal (beneath the serosa). Subserosal or submucosal tumors may be pedunculated and on long stalks. Submucosal tumors are prone to ulcerate resulting in severe menorrhagia. MR provides the best characterization of size, number, and location. Leiomyomas are usually low signal compared to myometrium on both T1WI and T2WI, although visualization is best on T2WI (Fig. 49.5). Areas of degeneration and cystic change cause inhomogeneous high internal signal. The tumors are well demarcated from adjacent myometrium by a discrete rim of low signal. Contrast enhancement does not improve leiomyoma detection or characterization. On CT, leiomyomas appear as homogeneous or heterogeneous masses that may be hypodense, isodense, or hyperdense relative to enhanced myometrium. Coarse calcifications within the mass are common and characteristic (Fig. 49.6). Cystic degeneration produces interior low density. Diffuse enlargement of the uterus and lobulation of its contour are common. Pedunculated leiomyomas may appear as adnexal rather than uterine masses. Lipoleiomyomas contain macroscopic fat detected on CT (Fig. 49.7), or by MR using fat-suppression sequences.

Adenomyosis is a benign disease of the uterus characterized by the presence of ectopic endometrial glands and stroma within the myometrium eliciting surrounding myometrial hypertrophy. Patients present with dysmenorrhea or menorrhagia. The disease may be focal or diffuse. MR provides the best detection of the disease. *Diffuse disease* is indicated by regular or irregular thickening of the junctional zone myometrium >12 mm. The low signal abnormality corresponds to myometrial hypertrophy. Half of the patients also demonstrate high signal foci within the myometrium corresponding to islands of endometrial glands with cystic change or hemorrhage (Fig. 49.8). *Focal disease* is evidenced by low signal masses within the myometrium on T2WI. These masses are isointense to myometrium on T1WI. High signal foci occasionally seen on T1WI represent hemorrhage. Differentiation from leiomyomas is difficult. Leiomyomas are characteristically well circumscribed while adenomyomas are poorly defined with vague margination. Adenomyosis is not routinely evident on CT. US findings are usually subtle and nonspecific.

Nabothian cysts are retention cysts of the mucous-secreting glands of the cervical epithelium. They are common, benign, and generally of no clinical significance. On MR they appear as bright, round, well-defined structures in the cervix on T2WI (Fig. 49.1A). On T1WI, they are isointense to urine or muscle. Small size and sharp margins differentiate nabothian cysts from *adenoma malignum*, a multicystic form of adenocarcinoma of the cervix. This malignancy appears as multicystic mass with numerous small cysts on a background of enhancing solid tissue.

Physiologic ovarian cysts and normal ovarian follicles contain simple fluid that is low signal on T1WI and high signal on T2WI. A uniform, thin, dark wall is evident on T2WI. Gadolinium enhancement of the cyst wall is common but not constant. On CT, they are well defined, thin walled, and have homogeneous internal density near water. Size less than 3 cm is indicative of physiologic ovarian follicle (Fig. 49.9). The corpus luteum is a normal physiologic ovarian structure that develops at the site of the dominant follicle following ovulation. A normal corpus luteum is smaller than 3 cm, and has a diffusely thick wall and prominent peripheral blood flow. A crenulated, collapsed cyst appearance is usual. Central hemorrhage is often present.

Hemorrhagic functional ovarian cysts appear high signal on T1WI if a large amount of methemoglobin is present. If predominantly intact red blood cells are present, the cyst appears low signal on T2WI. Thus hemorrhagic cysts may be low signal on both T1WI and T2WI, high signal on T1WI and low signal on T2WI, or low signal on T1WI and high signal on T2WI. Layering of blood products may be present. The absence of gadolinium enhancement differentiates internal blood clot adherent to the cyst wall from a solid nodule. On CT, hemorrhagic cysts appear as thin-walled cysts with internal density near water or higher in attenuation depending on the physical state of the blood products (Fig. 49.9). Atypical cysts can be followed with US to determine if they resolve after one or two menstrual cycles.

Endometriosis is the presence of endometrial tissue in locations outside of the uterus. The endometrial implants respond

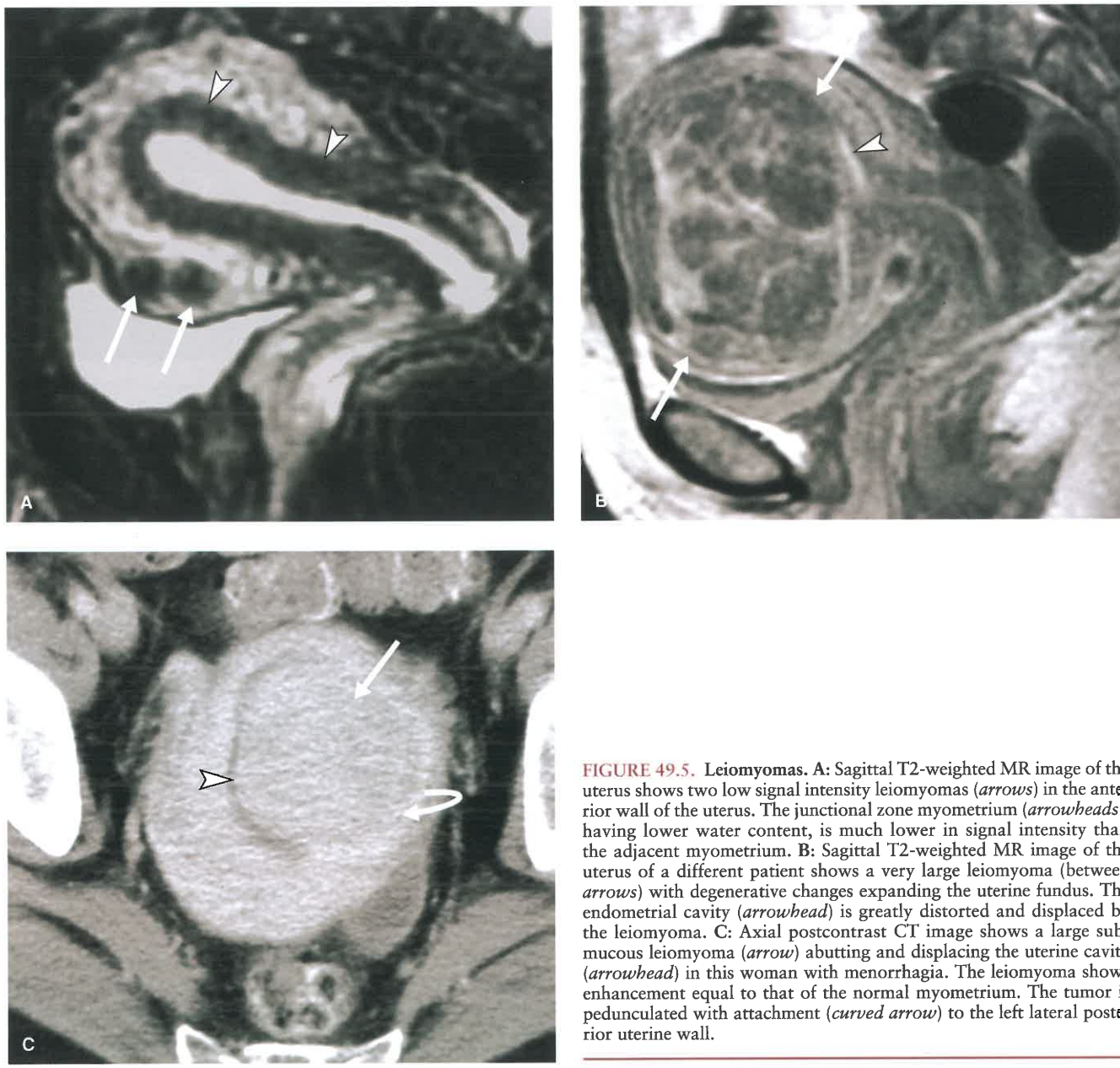

FIGURE 49.5. **Leiomyomas. A:** Sagittal T2-weighted MR image of the uterus shows two low signal intensity leiomyomas (*arrows*) in the anterior wall of the uterus. The junctional zone myometrium (*arrowheads*), having lower water content, is much lower in signal intensity than the adjacent myometrium. **B:** Sagittal T2-weighted MR image of the uterus of a different patient shows a very large leiomyoma (between *arrows*) with degenerative changes expanding the uterine fundus. The endometrial cavity (*arrowhead*) is greatly distorted and displaced by the leiomyoma. **C:** Axial postcontrast CT image shows a large submucous leiomyoma (*arrow*) abutting and displacing the uterine cavity (*arrowhead*) in this woman with menorrhagia. The leiomyoma shows enhancement equal to that of the normal myometrium. The tumor is pedunculated with attachment (*curved arrow*) to the left lateral posterior uterine wall.

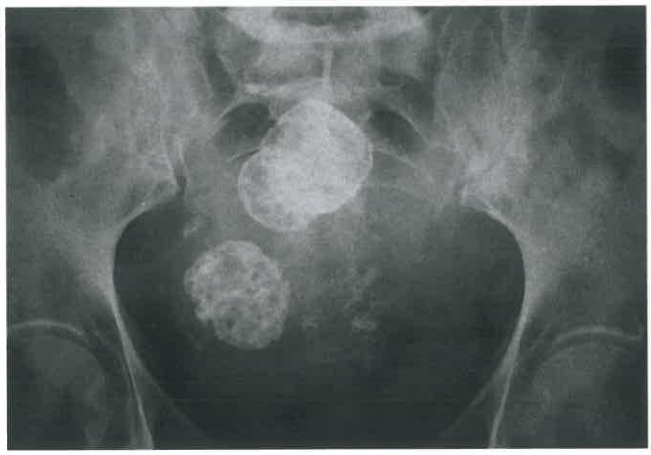

FIGURE 49.6. **Leiomyoma Calcifications.** Conventional radiograph of the pelvis reveals multiple leiomyomas with characteristic "popcorn" calcifications.

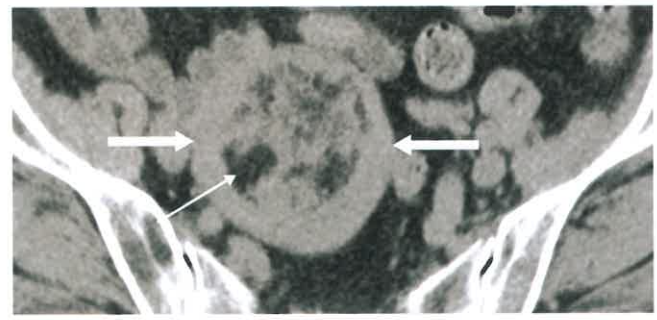

FIGURE 49.7. **Lipoleiomyoma.** Axial CT performed without contrast demonstrates a fat-containing myometrial tumor in the uterus (between *fat arrows*). Distinct fat attenuation (*skinny arrow*), equal to that of nearby pelvic fat, confirms the diagnosis of lipoleiomyoma.

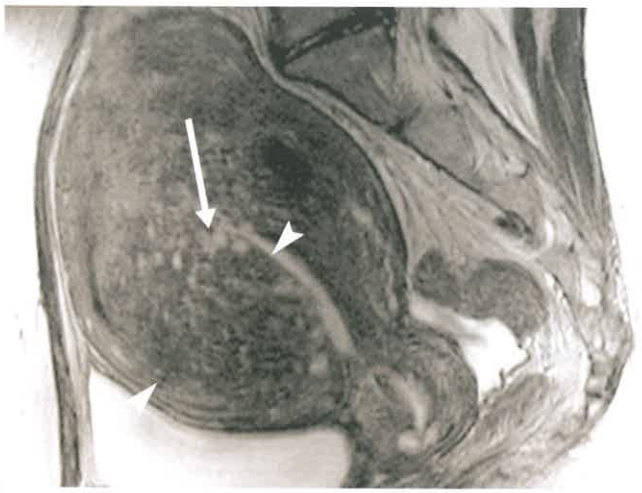

FIGURE 49.8. **Adenomyosis.** T2-weighted sagittal plane MR image shows marked widening of the junctional zone myometrium (between *arrowheads*), a key finding of adenomyosis. Tiny cystic deposits of endometrium seen as high signal intensity round foci (*arrow*) within the fibrotic lesion are also characteristic.

to cyclic hormonal stimulation resulting in recurrent bleeding, inflammation, and fibrosis. Hallmarks of disease include numerous tiny implantations of endometrial tissue on peritoneal surfaces, development of endometriomas (endometrial cysts filled with hemorrhage), and formation of adhesions between surrounding tissues. The most common sites of involvement are the ovaries, the cul-de-sac, and peritoneal reflections over the uterus, fallopian tubes, bladder, and rectosigmoid colon. All imaging modalities have high sensitivity for detection of endometriomas. Deep pelvic endometriosis is a cause of severe pelvic pain with tiny deposits of endometrium on peritoneal surfaces in recesses, pelvic organs, and other extraperitoneal sites. MR shows hypointense thickening and nodularity of ligaments and the walls of the vagina and rectum on T2WI. Endometriomas ("chocolate cysts") contain blood products of various ages reflecting recurrent episodes of bleeding corresponding to the menstrual cycle. They are characteristically multiple, bilateral, and located in the cul-de-sac. MR shows the cysts to be homogeneous high intensity on T1WI and characteristically low signal on T2WI, a finding termed "*T2 shading*" (Fig. 49.10). Loss of signal on T2WI is caused by the presence of methemoglobin within the cysts. Iron concentration and viscosity increase within the cysts as water is resorbed. The "shaded" fluid may layer dependently

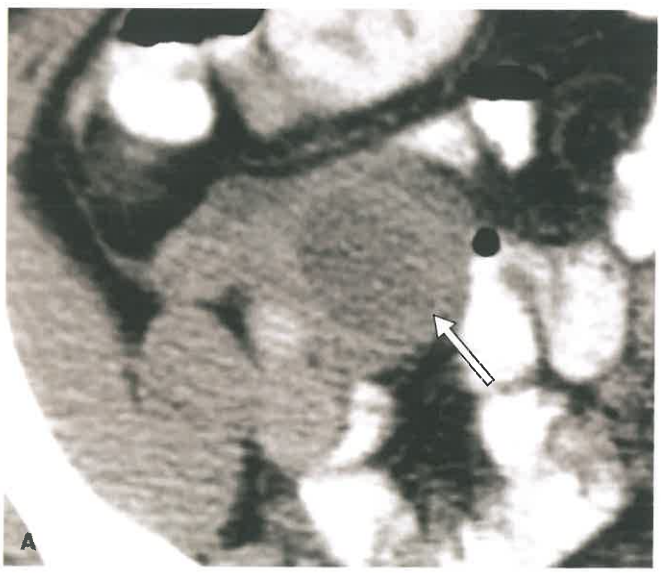

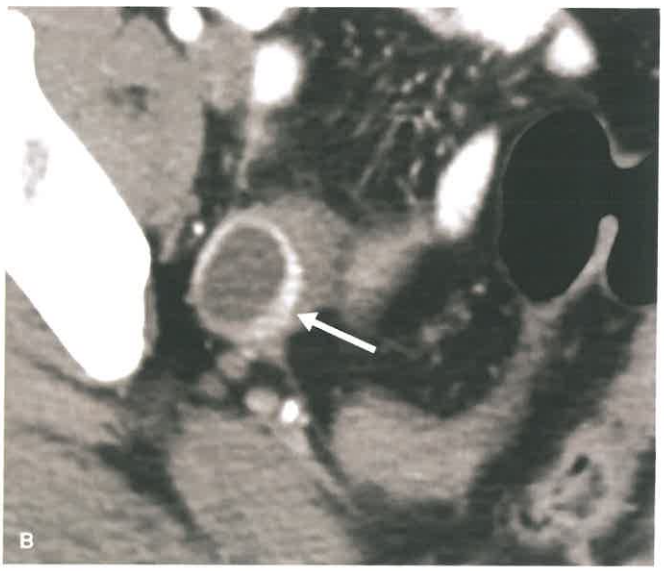

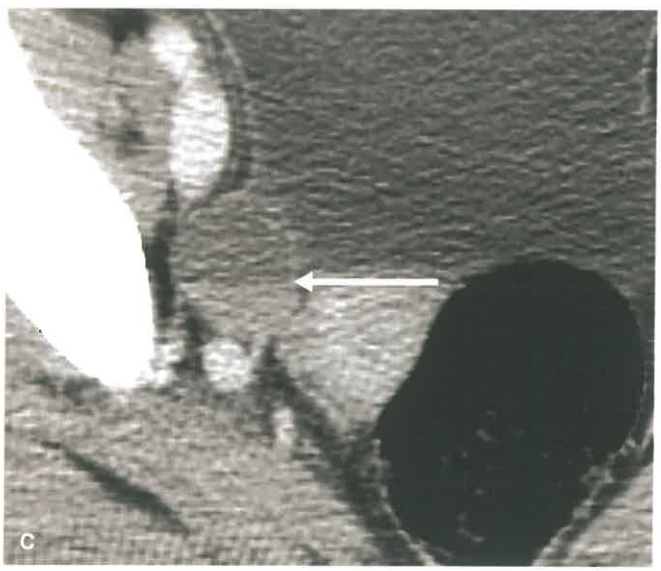

FIGURE 49.9. **Physiologic Ovarian Cysts. A:** Postcontrast CT reveals a thin-walled 2.6-cm cyst (*arrow*) arising from the right ovary in a 28-year-old woman. The appearance and size of this ovarian cyst are consistent with being a dominant follicle. This is a physiologic cyst and no follow-up is needed. **B:** Postcontrast CT in a 26-year-old woman shows an 18-mm right ovarian cyst (*arrow*) with intense rim enhancement. This appearance is consistent with a normal benign corpus luteum. A diagnosis of mittelschmerz was made after appendicitis was ruled out on this CT. **C:** Another CT performed for right lower quadrant pain in a 34 year old revealed a 3-cm right ovarian cyst with a fluid–fluid layer (*arrow*) yielding a diagnosis of hemorrhagic ovarian cyst as a cause for her pain. The dependent high attenuation fluid represents blood. Follow-up pelvic US in 10 weeks confirmed complete resolution.

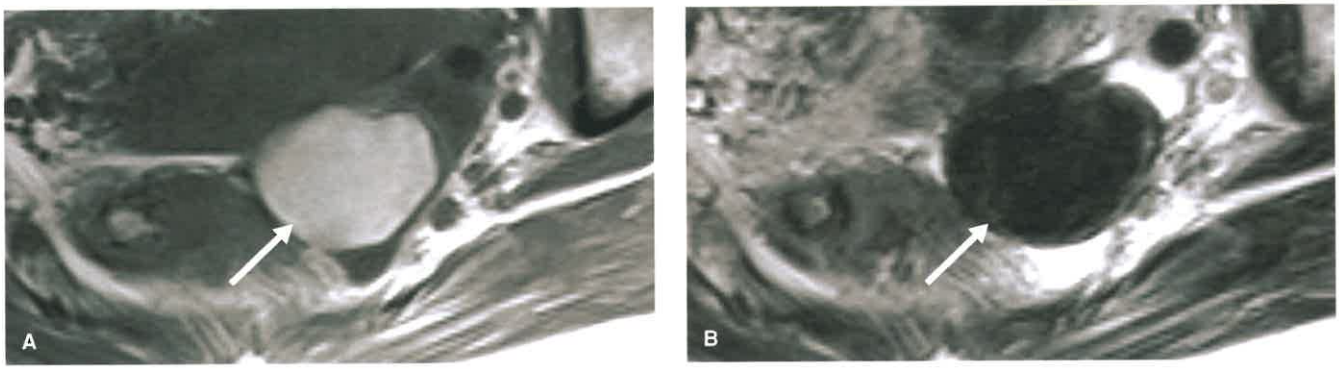

FIGURE 49.10. **Endometrioma—MR. A:** T1WI. **B:** T2WI. A cystic mass (*arrows*) in the cul-de-sac is high signal intensity on TIWI and shows characteristic loss of signal on T2WI (T2 shading). The loss of signal is caused by the presence of methemoglobin within the cyst resulting from multiple episodes of internal hemorrhage.

within the cyst. Cysts may appear heterogeneous because of the varying age of contained blood products. The cyst wall is usually low signal representing fibrous tissue or hemosiderin. Fat-saturation T1WI improves visualization of small implants on peritoneal surfaces. On CT, endometriomas appear as complex cystic pelvic masses, frequently with relatively high attenuation fluid components. Inflammation and fibrosis are prominent. Multiple pelvic organs may be incorporated into a mass. Hydrosalpinx is a common associated finding (30%). Endometriosis may involve bowel, the urinary tract, or occur outside the pelvis and in surgical scars. Malignant transformation of endometriosis is a rare occurrence.

Hydrosalpinx is a common adnexal mass that may occur as an isolated lesion or as a component of a complex adnexal mass. Occlusion of the fallopian tube, caused by infection, surgery, tumor, or endometriosis, results in fluid accumulation and dilatation of the tube. The most common cause is pelvic infection. Imaging of isolated hydrosalpinx demonstrates a sausage-, C-, or S-shaped adnexal structure distended with fluid of variable character that may be serous fluid, hemorrhage (hematosalpinx), or pus (pyosalpinx) (Fig. 49.11). Tortuosity, dilatation, and folding of the tube may resemble an ovarian tumor. Multiplanar images and identification of a normal ovary on the ipsilateral side assist in confirming the diagnosis. MR is sensitive to the nature of the fluid within the tube showing low signal on T1WI with high signal on T2WI for simple serous fluid. Proteinaceous fluid, hemorrhage, or pus causes high signal on T1WI. Pelvic inflammatory disease, endometriosis, or fallopian tumor may incorporate hydrosalpinx as a component of a complex cystic and solid adnexal mass. Hydrosalpinx is a common finding on HSG performed for infertility (Fig. 49.11A).

Pelvic inflammatory disease is a common affliction of women of reproductive age. The usual causative organisms are a mixture of anaerobic and aerobic bacteria from the vagina. Uncommon organisms include actinomycosis and tuberculosis. Endometritis and myometritis are treated medically. Imaging is performed to detect *tuboovarian abscess* and pyosalpinx, complications that may require surgical treatment. Early findings include pelvic and edema and stranding in the parametrium and paraovarian tissues. Pyosalpinx appears as a thick-walled edematous tube that contains complex fluid. Tuboovarian abscess appears as a thick-walled fluid-filled adnexal mass that incorporates the ovary and commonly a dilated fallopian tube (Fig. 49.12). Gas bubbles are occasionally present within the collection and are highly indicative of abscess. Adenopathy and ascites may be present.

Peritoneal inclusion cyst is an increasingly common and difficult to treat cause of chronic pelvic pain. Adhesions from previous surgery or inflammatory process entrap the ovary within a fluid collection that extends into peritoneal recesses. Continuing

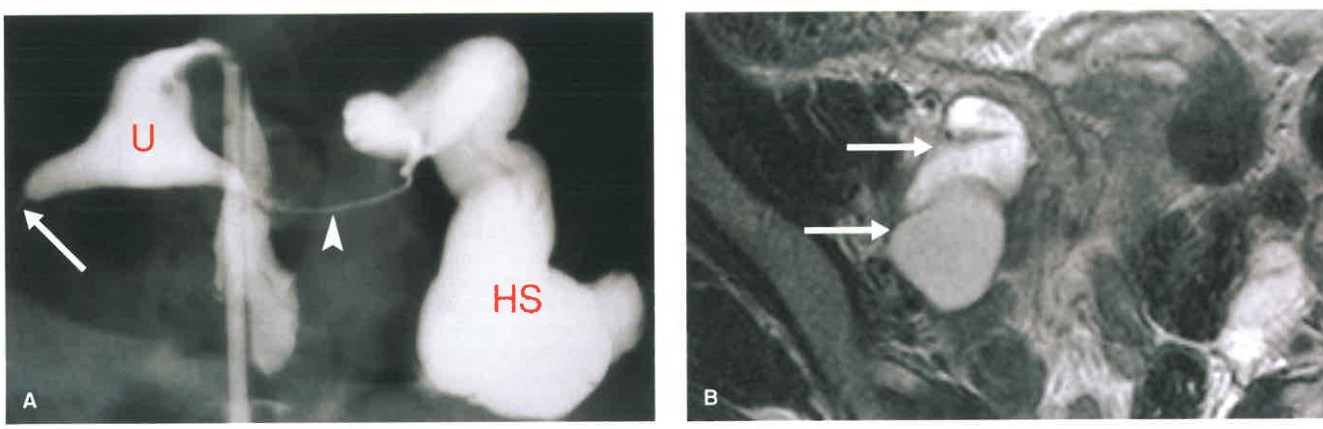

FIGURE 49.11. **Hydrosalpinx. A:** HSG demonstrates a retroflexed uterus (*U*) with the fundus directed posteriorly and inferiorly. The right fallopian tube is occluded at the isthmus (*arrow*). The left fallopian tube is massively dilated at its distal end, forming a hydrosalpinx (*HS*). The proximal portion (*arrowhead*) of the left fallopian tube is normal. No peritoneal spill of the injected contrast agent is present indicating bilateral total tubal occlusion. **B:** Axial T2-weighted MR in a different patient demonstrates a similar appearance of hydrosalpinx (*arrows*) as a dilated twisted convoluted tube on the right.

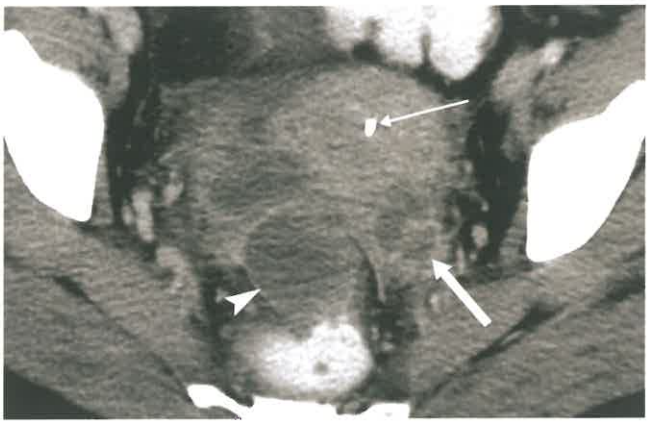

FIGURE 49.12. **Tuboovarian Abscess.** Postcontrast CT in a patient with fever, pelvic pain, and vaginal discharge shows a complex fluid collection enveloping the ovary (*fat arrow*), dilated fallopian tube (*arrowhead*), and uterus containing an IUD (intrauterine device) (*skinny arrow*). Note the extension of edema and inflammation into pelvic fat and the poor margination of involved organs. These are classic findings of tuboovarian abscess.

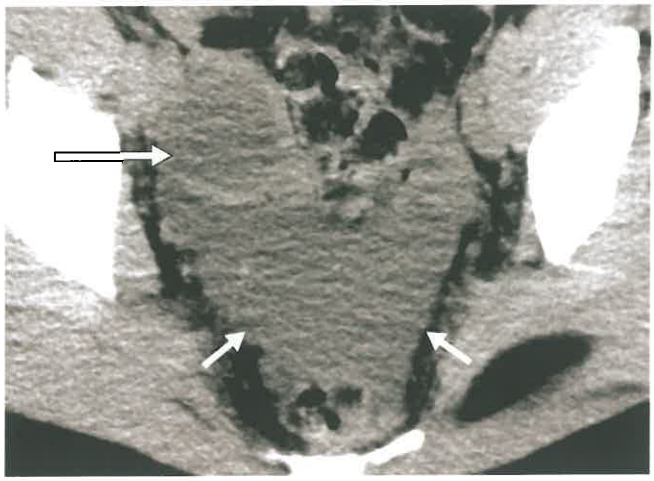

FIGURE 49.13. **Peritoneal Inclusion Cyst.** CT reveals a loculated fluid collection partially enveloping the right ovary (*large arrow*) and extending into the recesses of the peritoneal cavity (*small arrows*) in a patient with chronic pelvic pain. Attempts at needle and catheter drainage were unsuccessful. The patient became asymptomatic following oophorectomy.

secretion of fluid by the active ovary is not absorbed by the diseased peritoneal surfaces producing pain and pressure systems. Imaging shows a fluid collection that includes the ovary. The fluid is usually simple and characteristically extends into peritoneal recesses giving the collection an angled or pointed rather than spherical or oval shape (Fig. 49.13). Effective treatment generally requires removal of the ovary.

Benign cystic teratoma, ordermoid cyst, is the most common germ cell neoplasm of the ovary. Lesions contain mature elements derived from ectoderm, mesoderm, or endoderm resulting in a broad range of appearance. Mean patient age at discovery is 30 years. Most lesions are discovered incidentally while the patients are asymptomatic. The cysts are filled with liquid sebaceous material that is fat density on MR and CT. Internal contents include the Rokitansky nodule, which commonly includes hair, teeth, bone, or cartilage. US features are usually characteristic, but lesions may be discovered or further characterized by MR or CT. MR shows the sebaceous material as very high intensity on T1WI. Signal is usually decreased on T2WI approximating fat signal. Fat content is confirmed by in-phase and out-of-phase gradient recall images or frequency selective fat saturation images. CT demonstration of fat density within a cystic adnexal mass is definitive (Fig. 49.14). CT and conventional radiographs show bone and teeth formation within the mass. Atypical lesions mimic a wide variety of other adnexal pathology including ovarian malignancy.

Fibrotic ovarian tumors account for 4% of ovarian tumors. Because they are solid masses and are commonly associated with ascites (40% of cases), they may mimic ovarian cancers (Fig. 49.15). Tissue types include fibromas, thecomas, and fibrothecomas arising from ovarian stroma. Meigs syndrome is defined as the association of ascites and pleural effusion with an ovarian fibroma. The syndrome resolves following surgical removal of the tumor. US demonstrates a solid mass with poor sound transmission. CT shows a solid mass with minimal enhancement. MR shows a well-defined ovarian mass that is predominantly low signal on both T1WI and T2WI. Scattered high signal areas within the mass on T2WI represent focal edema or cystic change.

Adnexal torsion is a gynecologic emergency resulting from twisting of the ovary, fallopian tube, or most commonly both structures restricting blood supply. Failure to promptly relieve torsion and restore blood supply results in infarction. Patients

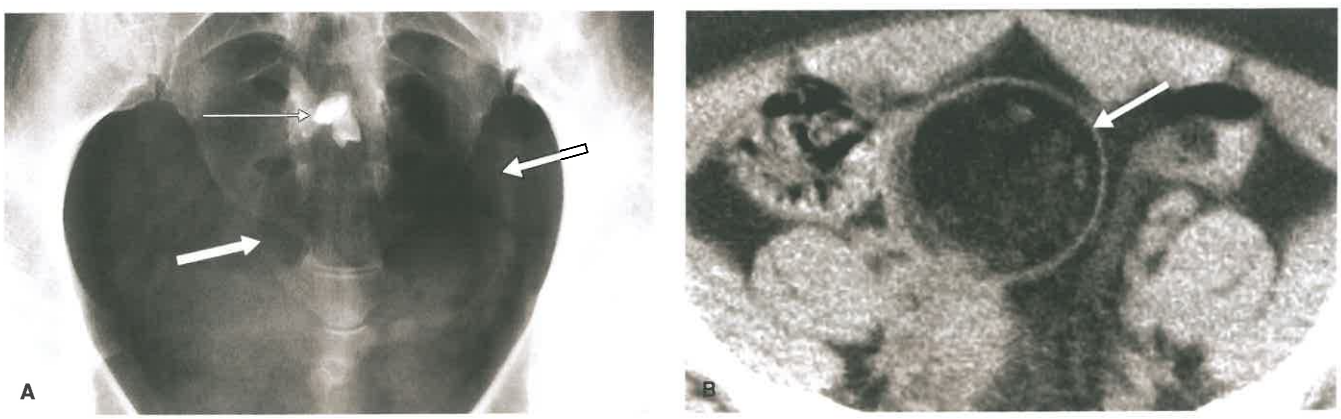

FIGURE 49.14. **Benign Cystic Teratoma. A:** Conventional radiograph of the pelvis in a young woman demonstrates several well-formed teeth (*skinny arrow*). A subtle, well-defined mass of fat density is also present (*fat arrows*). These findings are diagnostic of benign cystic teratoma. **B:** CT performed without contrast of a 28-year-old woman reveals a fat-density mass (*arrow*) diagnostic of a benign cystic teratoma.

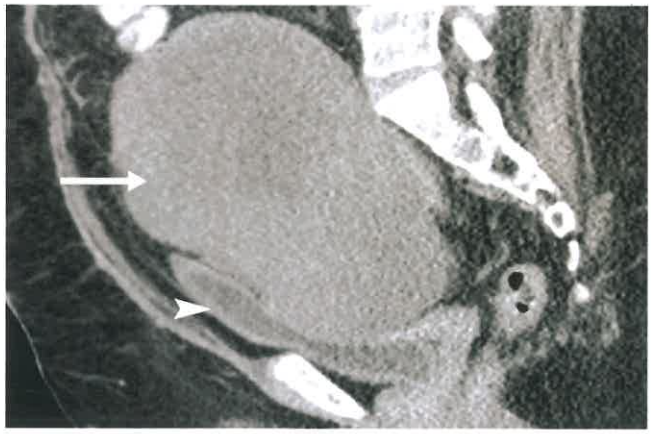

FIGURE 49.15. **Ovarian Fibroma.** Sagittal reformatted image from a CT scan demonstrates a very large lobulated homogeneous solid mass (*arrow*) arising from the pelvis and compressing the bladder (*arrowhead*). The patient had small pleural effusions and ascites that resolved after resection of the benign ovarian fibromas.

present with pain, nausea, vomiting, and leukocytosis. Diagnosis is most effectively made by US (see Figure 51.27). Key findings include a smooth-walled adnexal mass, which serves as a nidus for twisting (Fig. 49.16). The torsed mass demonstrates concentric wall thickening. The involved fallopian tube appears as an amorphous mass or as a tube with thickened walls. The uterus is deviated toward the torsed adnexa. Signs of hemorrhagic infarction of the torsed adnexa include marked thickening of the wall of the adnexal mass (>10 mm), hemorrhage within the mass and within the twisted tube, and hemoperitoneum.

Gynecologic Malignancy

Ovarian cancer represents 3% of all malignancy in women, but accounts for 15% of all cancer deaths. There are more than 20 histologic types of ovarian malignancy, however, epithelial (70%) and germ cell (15%) tumors account for the

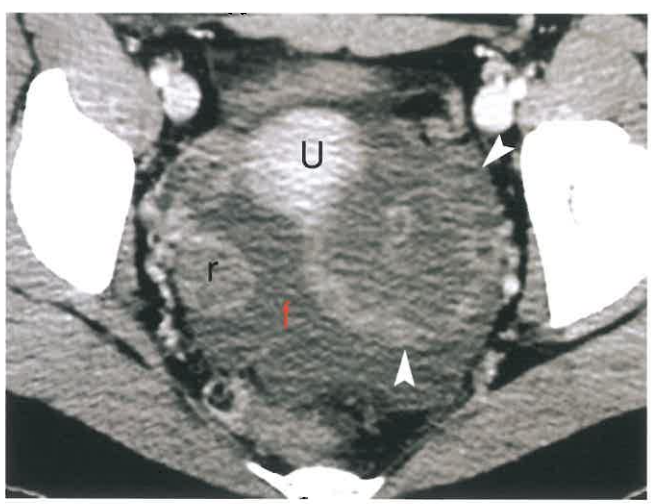

FIGURE 49.16. **Ovarian Torsion.** Axial postcontrast CT image shows a large cystic mass (*arrowheads*) arising from the left ovary with thickened poorly enhancing walls associated with a large volume of fluid (*f*) in the cul-de-sac. The patient was experiencing intermittent severe pelvic pain. Surgery reveals torsion of the left adnexa with a serous cystadenoma serving as the nidus for torsion. *U*, uterus; *r*, right ovary.

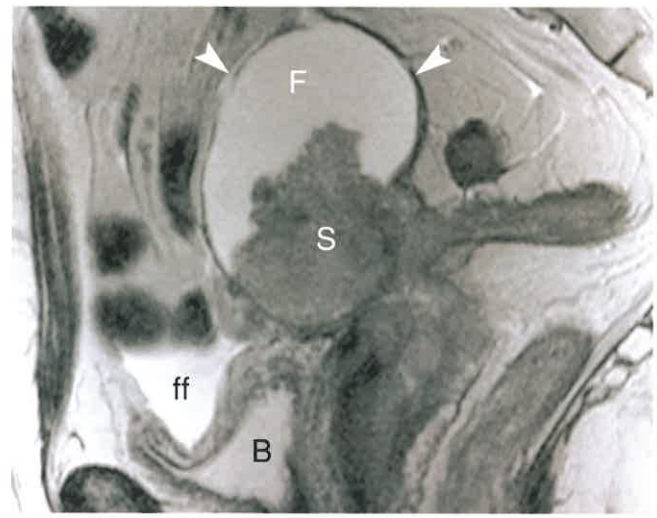

FIGURE 49.17. **Cystadenocarcinoma Ovary.** Sagittal plane MR T2WI in a 63-year-old woman demonstrates a cystic adnexa mass (*arrowheads*) with a prominent solid component (*S*) highly indicative of malignancy. The fluid content (*F*) of the mass was high signal on both T1WI and T2WI indicating internal hemorrhage or high protein content. Free intraperitoneal fluid (*ff*) is also present indicating high likelihood of intraperitoneal metastases. *B*, bladder.

majority. Approximately 40% of ovarian tumors are malignant, two-thirds are cystic, and 25% are bilateral. The peak age of onset of ovarian cancer is 55 to 59. Ovarian malignancy has an insidious onset and a silent growth pattern that results in advanced disease at presentation in 70% of cases. CA 125 is a serologic marker for ovarian cancer found to be elevated in 80% of women with ovarian cancer. Unfortunately, it is more likely to be abnormal in advanced cancers and is elevated in only 25% to 50% of stage I ovarian cancers. Survival correlates directly with the stage of disease, which also determines treatment. MR and CT signs of ovarian malignancy are similar to those listed for US in Chapter 51. Wall thickness greater than 3 mm, nodularity, vegetations, solid components, evidence of invasion of adjacent structures, ascites, contrast enhancement of the peritoneum, and adenopathy are evidence of malignancy (Fig. 49.17). Ovarian carcinoma spreads primarily by peritoneal seeding with small tumor nodules implanting on the peritoneum, mesentery, and omentum, and malignant ascites (Fig. 49.18). Secondary patterns of spread include direct extension to adjacent structures, lymphatic metastases to pelvic and retroperitoneal nodes, and late hematogenous spread to lung, liver, and bones. CT is used primarily for follow-up of known ovarian cancer. Because ovarian cancer is usually staged with surgical laparotomy, initial radiographic tumor staging is indicated only in clearly advanced cases. Initial treatment is total abdominal hysterectomy, bilateral salpingo-oophorectomy, omentectomy, and tumor debulking. Both CT and MR are relatively poor in the detection of peritoneal metastases. The presence of ascites is highly predictive of the presence of peritoneal metastases. A careful search for focal peritoneal thickening and tiny nodules should be conducted. Thickening of the bowel wall and distortion of bowel loops suggest intestinal involvement. No imaging method can reliably differentiate benign from malignant ovarian masses. This is not surprising because many cases are borderline malignant, even histologically.

Metastases to the ovary occur by peritoneal spread, direct extension, or hematogenous dissemination and account for 10% of ovarian malignancies. Most metastases to the ovaries originate as colon cancers (65%) with other common primary

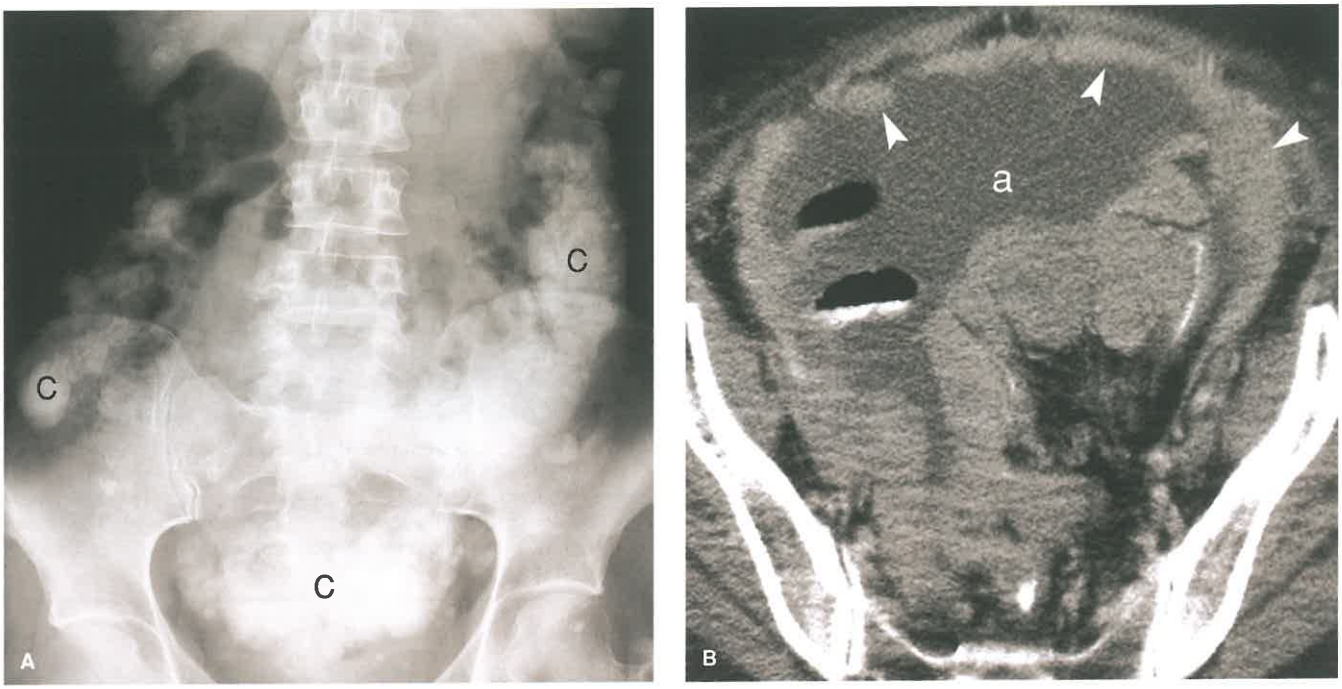

FIGURE 49.18. **Peritoneal Metastases From Ovarian Carcinoma. A:** Conventional radiograph of the abdomen demonstrates calcified implants of ovarian carcinoma (*C*) throughout the peritoneal cavity. The pathologic diagnosis was metastatic papillary serous cystadenocarcinoma of the ovary. **B:** CT image reveals nodular tumor implants (*arrowheads*) on the parietal peritoneum well outlined by ascites (*a*). The patient had metastatic ovarian carcinoma.

tumors being stomach, breast, lung, and pancreas. Most metastases are solid, bilateral, and enhance avidly. Cystic metastases are usually indistinguishable from ovarian primary tumors (Fig. 49.19). The term "Krukenberg tumor" is properly applied only to mucinous tumors metastatic to the ovary from a mucinous gastric carcinoma. Ovarian lymphoma produces large bilateral solid ovarian masses that show minimal enhancement.

Cervical cancer is the most common gynecologic malignancy. Squamous carcinoma accounts for 95% and adenocarcinoma for 5% of these cases. The peak age of onset is 45 to 55 years, but it is the second most common malignancy in women aged 15 to 34. Cervical cancer spreads predominantly by direct extension to involve the vagina, paracervical and parametrial tissues, and the bladder and rectum. Obstruction of the ureters is particularly common because of their proximity to the cervix. Lymphatic metastases to the pelvic, inguinal, and retroperitoneal nodes are common. Hematogenous metastases to the lung, bone, and brain occur only late in the course of the disease.

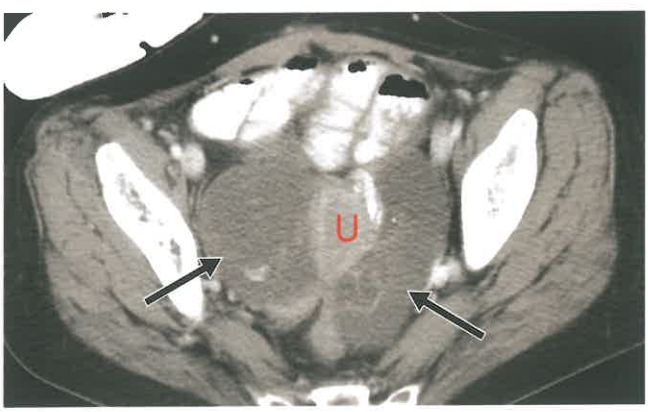

FIGURE 49.19. **Metastases to the Ovary.** Cystic metastases (*arrows*) replace and enlarge both ovaries compressing the uterus (*U*) in this patient with mucinous adenocarcinoma of the colon. The patient has had a colectomy and has an ileostomy bag.

MR is usually preferred to CT for staging of proven disease. On T1WI, cervical carcinoma is isointense with the myometrium. On T2WI, the tumor is higher in signal compared with the low signal of normal cervical tissue. A continuous rind of low signal cervical stroma surrounding the tumor is reliable evidence of the absence of parametrial invasion (Fig. 49.20). Signs of side wall invasion include tumor abutting or extending to within 3 mm of pelvic musculature. High-intensity signal in the parametrium on T2WI is evidence of parametrial invasion. Vaginal involvement is evidenced by loss of the normal thin rind of vaginal muscle on T2WI. Local staging by CT is limited by the fact that up to 50% of tumors are isodense to cervical tissue on both contrast and noncontrast scans (Fig. 49.21). Visible tumor is heterogeneously hypodense on postcontrast scans. Both MR and CT use node enlargement (>10 mm in short axis) as the primary criterion for involvement. This is inherently inaccurate because cervical cancer is known to involve nodes without enlarging them. Central necrosis within a lymph node is highly predictive of tumor involvement regardless of node size. Lymphatic spread involves internal and external iliac, presacral, and para-aortic nodes. Distant metastases most commonly involve liver, lung, and bone. Imaging studies should include the kidneys to assess for obstruction. PET-CT may prove to the optimal imaging modality to determine the extent of disease and to demonstrate residual or recurrent tumor. However, its use is impaired by pitfalls and artifacts, and its role in cervical cancer is not yet fully determined.

Endometrial carcinoma is now the most common invasive gynecologic malignancy. Histologically it is 95% adenocarcinoma and 5% sarcoma. The peak age at onset is 55 to 62 years, with postmenopausal vaginal bleeding as the key symptom. The tumor spreads initially by invasion into the

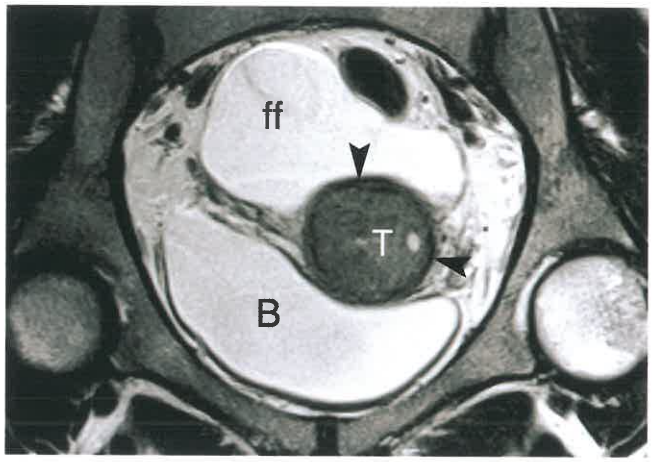

FIGURE 49.20. **Cervical Carcinoma—MR.** This T2-weighted MR image was obtained in an oblique coronal plane in order to image the cervix in transverse orientation. The tumor (*T*) appearing dark gray has nearly completely replaced the normal cervix seen only as a black rim (*arrowheads*). No parametrial invasion is evident. Free intraperitoneal fluid (*ff*) is seen in the cul-de-sac. *B*, bladder.

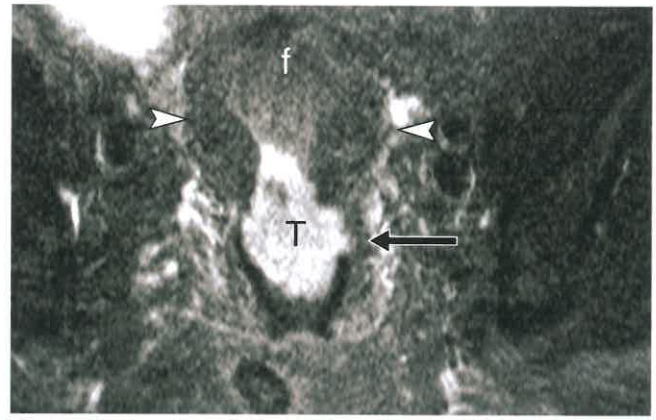

FIGURE 49.22. **Endometrial Carcinoma—MR.** Axial plane T2-weighted MR image through the uterus (between *arrowheads*) using fat saturation shows endometrial carcinoma (*T*) invading more than 50% of the thickness of the myometrium (*arrow*). This tumor is distinctly high signal compared to myometrium on this T2WI. *f*, fundus of the uterus.

myometrium and cervix, followed by lymphatic spread to the pelvic and retroperitoneal nodes, then continued direct spread into the broad ligaments, parametrium, and ovaries. Peritoneal seeding will occur with penetration of the uterine serosa. Hematogenous spread to the lung, bone, liver, and brain occurs late in the course of the disease. Prognosis and treatment depend on stage of the disease with the most critical factors being the depth of myometrial invasion and the involvement of lymph nodes. Lymph node metastases are unlikely if myometrial invasion is less than 50%. MR staging is more accurate than CT staging. On MR, the signal from tumor is similar to that of endometrium. Tumor is isointense to myometrium on T1WI and hyperintense to myometrium on T2WI (Fig. 49.22). Evidence of tumor includes thickening and poor definition of the endometrium. Large tumors appear as a polypoid mass that expands the uterine cavity. Tumor enhancement with gadolinium is variable and may be less than or greater than enhancement of myometrium and endometrium. Invasion of myometrium is determined on postcontrast T2WI. An intact junctional zone myometrium is evidence of the absence of myometrial invasion. Pitfalls for myometrial invasion include thinning of the myometrium by rapidly expanding tumors. Cervical invasion is determined on sagittal T2WI and postcontrast sequences with enhancing tumor seen within the dark tissue of the cervix. T1WI shows parametrial invasion into fat. Invasion of the bladder and rectum is evidenced by disrupted tissue planes and tumor signal with bladder or rectal wall on T2WI. On CT, the depth of myometrial invasion is determined on postcontrast images. The tumor enhances less than myometrium (Fig. 49.23). Obstruction of the cervix results in filling of the uterine cavity with fluid of variable density. Cervical involvement appears as heterogeneous enlargement of the cervix. Parametrial invasion appears as irregular margins of the uterus, parametrial soft tissue stranding, or parametrial mass. CT and MR evidence of nodal metastases are lymph nodes larger than 10 mm in short axis.

Uterine sarcomas are the most aggressive of the uterine tumors. Sarcomas may be suspected when uterine masses are large and heterogeneous. Malignant *mixed Müllerian tumors* are large solid tumors with prominent necrosis and hemorrhage that expand the uterine cavity and invade the myometrium. They appear as an intracavitary mass. Lymphatic and peritoneal spread are common. *Leiomyosarcomas* usually present as a rapidly growing pelvic mass. The uterus is

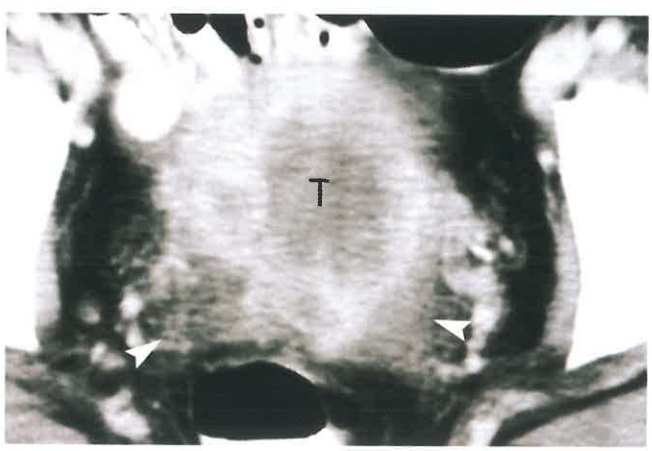

FIGURE 49.21. **Cervical Carcinoma—CT.** Heterogeneous tumor (*T*) has completely replaced the cervix on this CT scan. Stranding densities (*arrowheads*) into the paracervical fat indicate parametrial invasion by tumor.

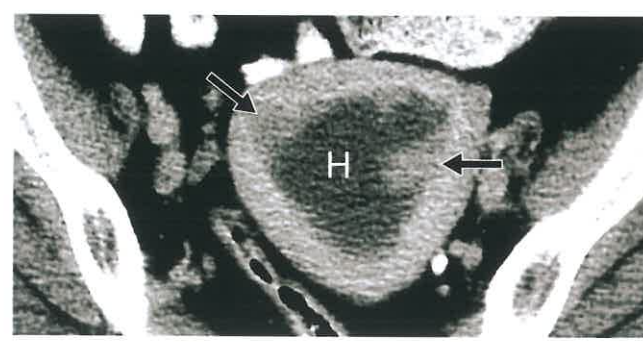

FIGURE 49.23. **Endometrial Carcinoma—CT.** Postcontrast CT image shows enhancing tumor nodules (*arrows*) invading the myometrium and extending into the uterine cavity being partially outlined by low attenuation hemorrhagic fluid (*H*). Tumor invasion is difficult to assess because the tumor is nearly isointense with enhanced myometrium.

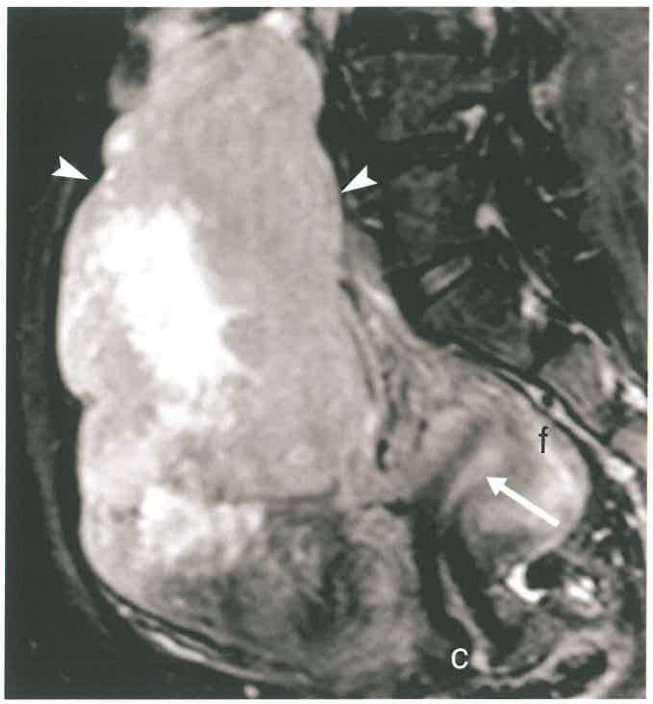

FIGURE 49.24. **Leiomyosarcoma.** T2WI shows a huge heterogeneous tumor mass (*arrowheads*) arising from the anterior wall of the retroflexed uterus. Note that the uterine cavity (*arrow*) is intact. The exophytic myometrial origin and heterogeneity of the mass are indicative of either a degenerated leiomyoma or a leiomyosarcoma. The latter diagnosis was confirmed at surgery. *f*, fundus of the uterus; *c*, cervix.

enlarged with a markedly heterogeneous mass with extensive necrosis, hemorrhage, and frequent calcifications (Fig. 49.24). Imaging differentiation from a degenerated benign leiomyoma is not possible unless signs of malignant spread of tumor are evident. *Endometrial stromal sarcomas* appear as polypoid endometrial masses that invade the myometrium.

Fallopian tube carcinoma is very rare accounting for only about 1% of gynecologic malignancy. Tumor types include serous adenocarcinoma, endometrioid carcinoma, and transitional cell carcinoma. Most tumors arise in the ampulla and occlude the tube causing hydrosalpinx (Fig. 49.25). Most

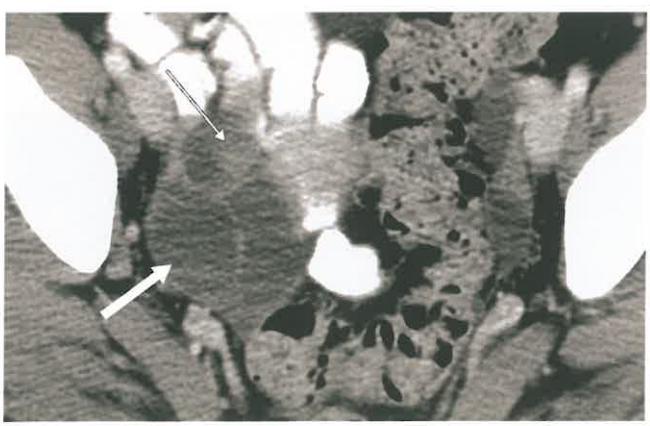

FIGURE 49.25. **Carcinoma of the Fallopian Tube.** Postcontrast CT shows a right sided hydrosalpinx (*fat arrow*). Close inspection reveals a papillary soft tissue attenuation nodule (*skinny arrow*) within the lumen of the dilated tube. Surgical resection confirmed adenocarcinoma of the fallopian tube.

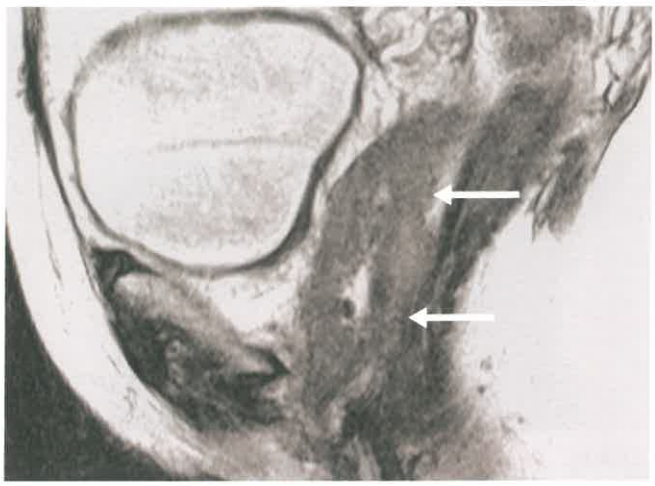

FIGURE 49.26. **Carcinoma of the Vagina.** Sagittal T2-weighted MR in a patient with previous hysterectomy shows marked nodular circumferential thickening (*arrows*) of the entire vagina. Biopsy revealed adenocarcinoma.

tumors are small. On MR, the small solid lesions are low signal on T1WI and high signal on T2WI. Most show enhancement with intravenous contrast administration. Fluid in the distended tube is usually complex reflected by high signal on T1WI.

Vaginal malignancies are also rare accounting for another 1% of gynecologic malignancies. Most are squamous cell carcinomas (85%) usually arising from the posterior wall of the upper third of the vagina. The remaining tumor types are adenocarcinoma, melanoma, and sarcoma. The vagina is much more commonly involved by direct spread of cervical, uterine, or rectal cancers. Primary vaginal malignancies produce a circumferential constricting lesion of the vagina (Fig. 49.26) or an ulcerated mass. MR shows low signal on T1WI and intermediate signal on T2WI. Use of vaginal gel during MR imaging greatly improves tumor visualization.

MALE GENITAL TRACT

Testes and Scrotum

US, supplemented by color Doppler, remains the initial imaging method of choice to evaluate the testes and scrotal contents. MR using surface coils offers excellent spatial resolution, greater tissue contrast, and wider field of view, but has the disadvantages of greater cost and lesser availability. MR is the choice for additional characterization of scrotal lesions when US findings are insufficient to determine for treatment. CT is the imaging method of choice for the staging of testicular neoplasms and in locating undescended testes that are not found by US. MR offers a staging alternative to CT. Radionuclide imaging provides useful information about perfusion, but with limited anatomic detail. This chapter reviews MR and CT imaging. Scrotal US is reviewed in Chapter 51.

Normal MR Anatomy. Because of high fluid content, the testes are of uniform low to intermediate signal on T1WI and uniform high signal on T2WI (Fig. 49.27). The tunica albuginea forms a well-defined 1 mm thick rim low in signal on T1WI and T2WI. Testicular masses are well depicted as lower in signal intensity than the bright testicular parenchyma on T2WI. Septations are often visualized radiating from the mediastinum to the tunica albuginea. A small amount of fluid is normally present in the

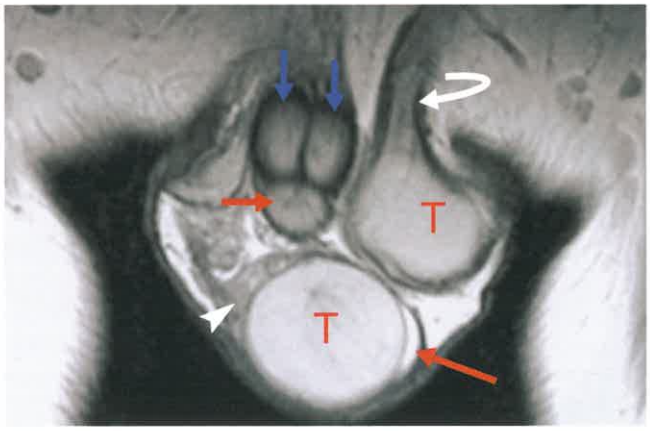

FIGURE 49.27. **Normal MR Anatomy: Male.** Coronal plane T2-weighted MR shows both testes (*T*) and the penis in cross-section. The testes are high in signal because of their high fluid content. The epididymis (*arrowhead*) is also high signal on T2WI but less than that of the testes. The left testis is suspended on the spermatic cord (*curved arrow*). The paired corpora cavernosa (*blue arrows*) are well demonstrated. The corpus spongiosum (*red arrow*) contains the urethra. A small amount of fluid (*long red arrow*) is present between the layers of the tunica vaginalis.

scrotum between the layers of the tunica vaginalis. The epididymis is isointense to the testes on T1WI and brightens on T2WI, though to a lesser extent than the testis. Postcontrast images depict homogeneous enhancement of the testis and avid hyperenhancement of the epididymis. The scrotum is intermediate signal reflecting the dartos muscle. The spermatic cord appears as numerous tubular structures representing the arteries and veins with MR signal determined by blood flow.

Undescended Testis. CT and MR are used to localize undescended testes not demonstrated by US to be within the inguinal canal. The testis, if present, will be seen between the lower pole of the kidney and the internal inguinal ring. In 3% to 5% of cases, the testis is congenitally absent. The undescended testis appears as an oval soft tissue mass up to 4 cm in size (Fig. 49.28). Because the undescended testis is usually atrophic, MR may show low or intermediate, instead of high signal, on T2WI. Undescended testis in the adult may be complicated by testicular tumor.

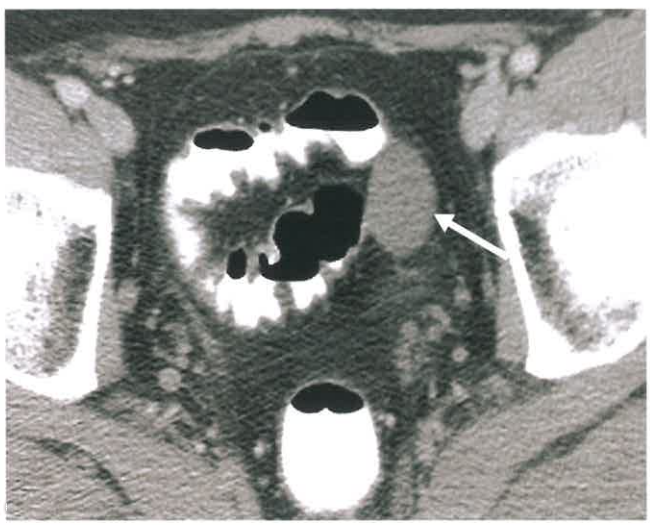

FIGURE 49.28. **Undescended Testis.** An undescended left testis (*arrow*) is found in the pelvis of a 40-year-old male. The testis is mildly atrophic.

Neoplasms. Diagnosis of testicular neoplasms is made by physical examination and US. The primary tumor in the testis may be clinically occult, yet is effectively demonstrated by US. Only in the rare case of an indeterminate lesion on US will MR of the testis be performed for further characterization. On MR, seminomas (60% of germ cell neoplasms) are homogeneous and hypointense to normal testis on T2WI. Nonseminomatous germ cell neoplasms (40%) are heterogeneous with areas of necrosis and hemorrhage but are still primarily low signal to normal testis on T2WI. Both tumor types enhance moderately showing prominent fibrovascular septa. Lymphoma, seen primarily in men >60 years, replaces testicular parenchyma with infiltrative tumor low in signal on T1WI and T2WI, and with low-level enhancement. Neither US nor MR can reliably differentiate benign from malignant testicular tumors.

With current treatment methods 95% of patients with germ cell testes neoplasms can be cured. Selection of proper treatment depends on staging, which relies primarily on CT, though MR offers an alternative accurate staging method. Lymphatic spread of tumor is most common, with a usual pattern of orderly ascending nodal involvement. Initial spread is along gonadal lymphatic vessels following the testicular veins to renal hilar nodes. Lymphatic metastases may also follow the external iliac chain to the para-aortic nodes. The internal iliac and inguinal nodes are rarely involved. Extensive metastatic involvement of the lymph nodes mimics lymphoma in young males. Hematogenous spread to the lungs usually follows lymphatic spread, except with choriocarcinoma, which spreads hematogenously early.

Scrotal Fluid Collections. Simple hydroceles show signal characteristics of water, low signal on T1WI and high signal on T2WI. Hematoceles and pyoceles show high signal on T1WI, reflecting complex fluid and high protein content. *Epididymal cysts* show the signal of simple fluid. *Spermatoceles* commonly contain fat and high protein causing high signal on T1WI, and layering debris may be evident. *Varicoceles* appear as serpiginous tubular structures in the spermatic cord. Signal intensity corresponds to slow blood flow. CT shows hydroceles as low attenuation fluid within the scrotum and varicoceles as enhancing tubular structures (Fig. 49.29).

Epididymitis/Orchitis. Orchitis causes inhomogeneous signal on both T1WI and T2WI, indistinguishable from tumor. With epididymitis, the epididymis is enlarged but signal intensity on T2WI is unpredictable and may be increased, decreased, or normal. Dilated vessels in the spermatic cord reflect hypervascularity. Hydrocele is usually present. Inflamed tissue shows avid enhancement.

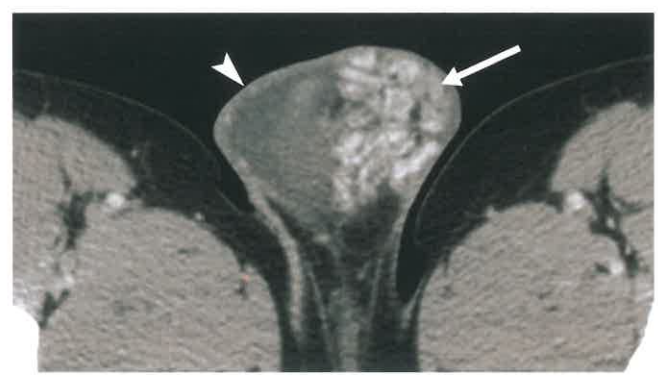

FIGURE 49.29. **Varicocele and Hydrocele.** Axial postcontrast CT through the scrotum reveals a large hydrocele (*arrowhead*) on the right and a very large enhancing varicocele (*arrow*) on the left.

Testicular torsion is best evaluated with Doppler US or scintigraphy. With acute torsion, MR may demonstrate a characteristic twisted pattern of torsion of the spermatic cord with impaired blood flow evident. The testis appears heterogeneous on all image sequences. Enhancement is diminished if blood flow is currently compromised but is intense if detorsion has occurred.

Prostate

Multiparametric MRI (mp-MRI) of the prostate has revolutionized imaging for detection and staging of prostate cancer. In 2012, the European Society of Urogenital Radiologists (ESUR) developed prostate MR imaging guidelines and suggested a PI-RADS (Prostate Imaging Reporting and Data System) structured reporting system. PI-RADS has been further refined by international consensus to version 2. Further refinement of this standardized reporting system is expected.

Current use of mp-MRI consists of a combination of high-resolution T2WI to assess anatomy with diffusion-weighted MRI (DWI) and MR spectroscopic imaging (MRSI) to improve specificity of lesion detection. Dynamic contrast-enhanced MRI (DCE-MRI) with gadolinium administration provides highly sensitive cancer detection. Each imaging method is assigned a PI-RADS score from 1 to 5 based on imaging findings and location. PI-RADS 1 indicates clinically significant cancer is highly unlikely. PI-RADS 2 indicates clinically significant cancer is unlikely. PI-RADS 3 indicates clinically significant cancer is equivocal. PI-RADS 4 indicates clinically significant cancer is likely. PI-RADS 5 indicates clinically significant cancer is highly likely. Recommendations for treatment are based on overall PI-RADS scoring. The details of PI-RADS scoring are complex and beyond the scope of this basic review. The reader is referred to Suggested Readings.

CT has no current role in the detection of prostate cancer as CT findings of benign and malignant disease overlap extensively. CT is also inferior to MRI for the staging of prostate cancer beyond the prostate. Transrectal US (TRUS) is used primarily to guide biopsy of areas of the prostate considered suspicious for cancer. However, TRUS underestimated the grade and the extent of prostate cancers. The role of PET-CT in prostate cancer is limited by the low metabolic activity of the tumor and high normal radionuclide activity in the bladder obscuring the prostate gland and surrounding tissues. Elevated serum prostate-specific antigen (PSA) (>3 to 4 ng/mL) has low specificity for prostate cancer, only 36%. A normal PSA does not exclude the presence of prostate cancer. These factors support the current enthusiasm for mp-MRI.

Normal MR Anatomy. The prostate is divided into three glandular zones surrounding the urethra (Fig. 49.30). The *peripheral zone* contains approximately 70% of prostate tissue and is draped around the remainder of the gland like a catcher's glove holding a baseball. Most prostate cancers (70%) arise in the peripheral zone. The *transitional zone* consists of two small areas of periurethral glandular tissue. Although it contains only 5% of prostatic tissue in the normal young man, it is the site of benign prostatic hypertrophy and may enlarge greatly in the older man. The *central zone* consists of the glandular tissue at the base of the prostate through which course the ducts of the vas deferens and seminal vesicles and the ejaculatory ducts. Although the central zone makes up 25% of glandular tissue, only 10% of cancers arise there. The anterior portion of the prostate is occupied by nonglandular tissue called the anterior *fibromuscular stroma.* The *base* of the prostate is that portion adjacent to the base of the bladder and the seminal vesicles (base to base). The *apex* of the prostate rests on the urogenital diaphragm. Prominent veins are frequently visualized in the periprostatic tissues. Lymphatic drainage of the prostate goes to regional pelvic lymph nodes with channels to para-aortic and inguinal nodes. Periprostatic venous connections to vertebral veins offer a route for the hematogenous spread of tumor to the axial skeleton. On T1WI, the prostate gland is uniform intermediate to low signal similar to skeletal muscle. The high signal periprostatic fat defines the margin of the prostate. Periprostatic veins and neurovascular bundles are low signal. On T2WI, the internal structure (zonal anatomy) of the prostate is demonstrated (Fig. 49.31). The peripheral zone is high in signal due to higher water content and looser acinar structure. The central zone is lower in signal due to more compact muscle fibers and acinar structure. The central and transitional zones become heterogeneous with age and the development of benign prostatic hyperplasia (BPH). The anterior fibromuscular stroma is low in signal and has poorly defined margins.

Normal CT Anatomy. The prostate gland is seen at the base of the bladder, just posterior to the symphysis pubis, as a homogeneous rounded soft tissue organ up to 4 cm in maximal diameter. Prostate zonal anatomy is not demonstrated by CT. A well-defined plane of fat separates the prostate from the obturator internus muscle.

Prostate carcinoma is the third leading cause of cancer death in men. Approximately one in six men will develop clinical prostate carcinoma in their lifetime. Despite the high prevalence and importance of prostate disease, treatment remains controversial. The primary issue is differentiating lethal from nonlethal disease. Nearly 50% of men older than 75 years of age will have prostate carcinoma on biopsy or autopsy. However, many of these cancers will not affect the patient's life span. The tumor is uncommon before age 50 and increases in incidence thereafter. The Gleason histologic grading system is used to assess the degree of differentiation of the tumor. A grade 1 is well differentiated and a grade 5 is anaplastic. The Gleason score varies from 2 to 10 and adds the Gleason grade for the predominant and the secondary portions of the tumors. Most tumors are adenocarcinoma (95%). Prostate cancer spreads

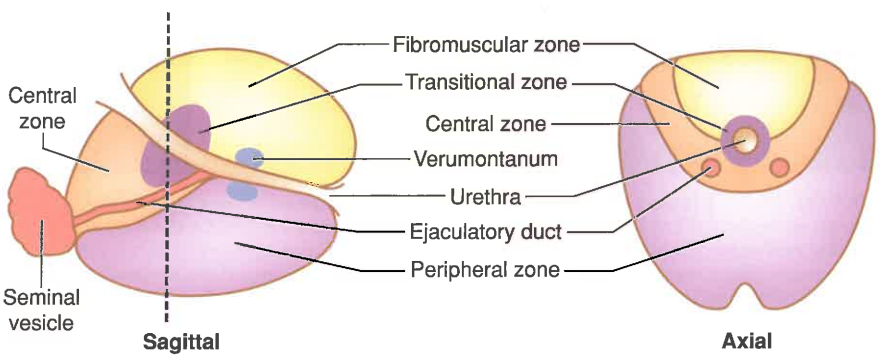

FIGURE 49.30. **Zonal Anatomy of the Prostate.** The anatomy is illustrated in midsagittal plane (*left*) and axial plane (*right*) at the level of the vertical *dashed line* on the left.

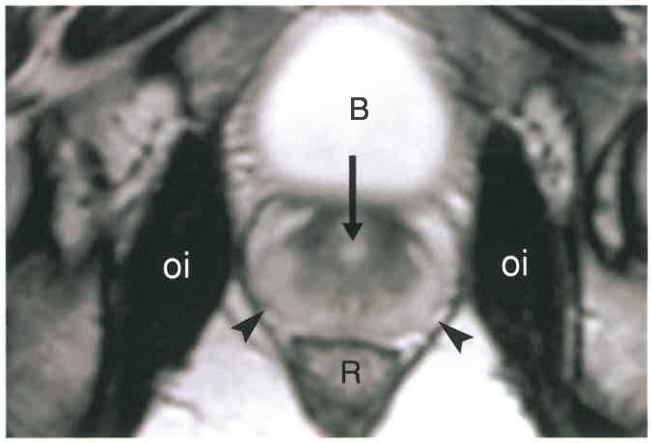

FIGURE 49.31. **Normal Prostate—MR.** Axial plane T2-weighted MR of a normal prostate in a 40-year-old man demonstrates the high-intensity peripheral zone (*arrowheads*), the urethra (*long arrow*), and the lower-intensity transitional zone surrounding the urethra. *B*, bladder; *r*, rectum; *oi*, obturator internus muscle.

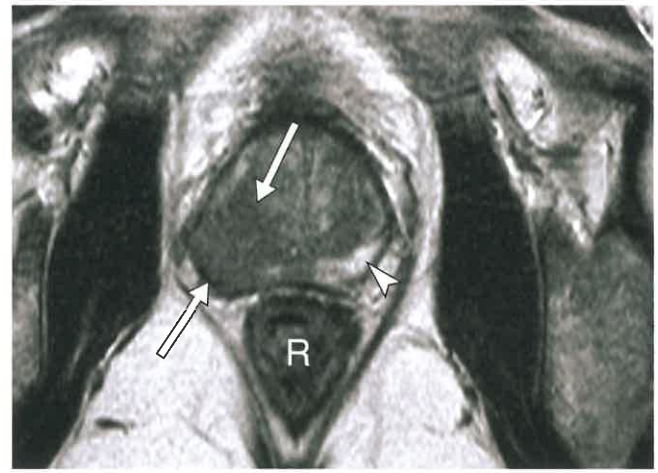

FIGURE 49.32. **Prostate Carcinoma.** Axial T2-weighted MR image of the prostate shows a low signal intensity adenocarcinoma (between *arrows*) replacing most of the peripheral zone and extending into the central gland of the prostate on the right. The peripheral zone on the left (*arrowhead*) remains normal high signal intensity. *R*, rectum.

by local extension, lymphatic vessels to regional nodes, and by hematogenous dissemination. Involvement of lymph nodes by metastatic disease is unreliably detected by conventional MR or CT because 70% of involved lymph nodes are small (<8 mm). Penetration of tumor through the capsule or into the seminal vesicles greatly worsens the prognosis. Involvement of the axial skeleton by hematogenous metastases is common. Metastases to the lungs, liver, and kidneys occur in the terminal phases of the disease.

On MR T2WI, cancers appear as areas of ill-defined low signal within the high signal peripheral zone (Fig. 49.32). Prostatitis, hemorrhage, scars, and posttreatment changes may have a similar appearance. In the transitional zone tumors are more difficult to detect overlapping the normal signal characteristics of transitional zone tissue. Cancer appears as an indistinct mass with homogeneous signal intensity, an appearance described as the "erased charcoal sign." Water-drop or lenticular shape is typical. Signal intensity is lower with high-grade cancers than with low-grade cancers. Criteria for extracapsular extension on T2WI include irregularity and thickening of the neurovascular bundle, loss of capsular enhancement, loss of visualization of the capsule, focal bulges of the capsule, and obliteration of the angle between the rectum and prostate. Prostate cancer shows intense early enhancement and variable early washout on DCE-MRI. On DWI, cancers show markedly hypointense focal abnormality on calculated apparent diffusion coefficient (ADC) maps and markedly hyperintense foci on high–*b*-value images. MRSI shows cancers have lower levels of citrate and higher levels of choline than benign prostate tissue. On T1WI, cancers are isointense with benign prostate tissue. T1WI is best used for assessing invasion of periprostatic fat and for detecting enlarged lymph nodes.

Benign prostatic hyperplasia begins at near age 40 and eventually occurs in all men. Hypertrophy and hyperplasia occur in glandular tissue in the transitional and periurethral zones accompanied by proliferation of supporting smooth muscle and stromal cells. The end result is focal or diffuse enlargement of the prostate (Fig. 49.33). Pressure on the

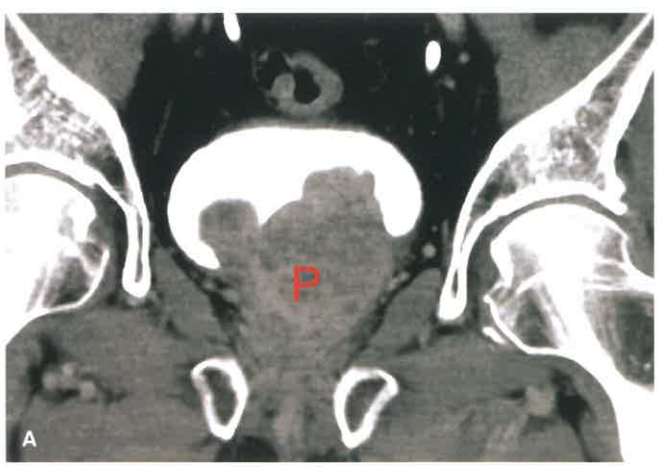

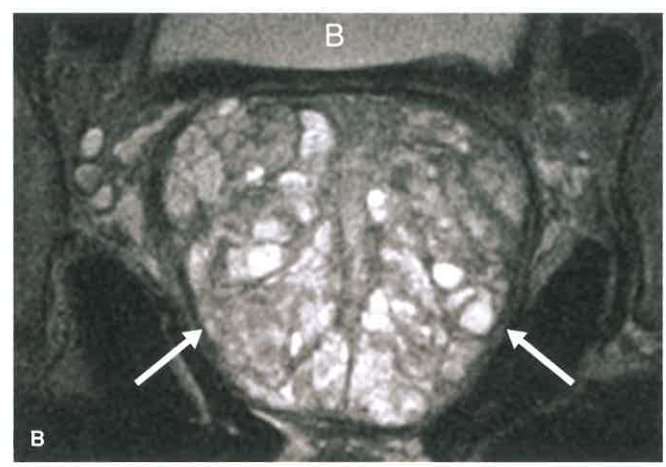

FIGURE 49.33. **Benign Prostatic Hypertrophy. A:** Postcontrast CT scan reformatted into coronal plane reveals marked nodular enlargement of the prostate gland (*P*) uplifting the bladder base. Despite marked hypertrophy of the prostate the bladder wall is only minimally thickened and the patient had only mild bladder outlet obstruction symptoms illustrating the clinical point that it is not the overall size of the prostate that matters but exactly where the hypertrophy occurs and how much narrowing of the urethra that it causes. **B:** T2-weighted MR image in axial plane shows marked diffuse enlargement of the prostate gland (*arrows*) with heterogeneous signal, nodules, and cystic change. The normal zonal anatomy of the prostate is not evident. *B*, bladder.

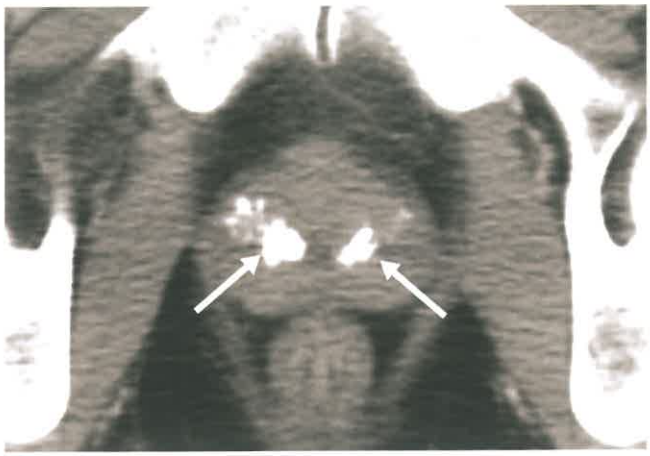

FIGURE 49.34. **Prostate Calcifications.** Axial postcontrast CT shows a mildly enlarged prostate with prominent coarse calcifications (*arrows*) typical of calcification associated with benign prostate hypertrophy.

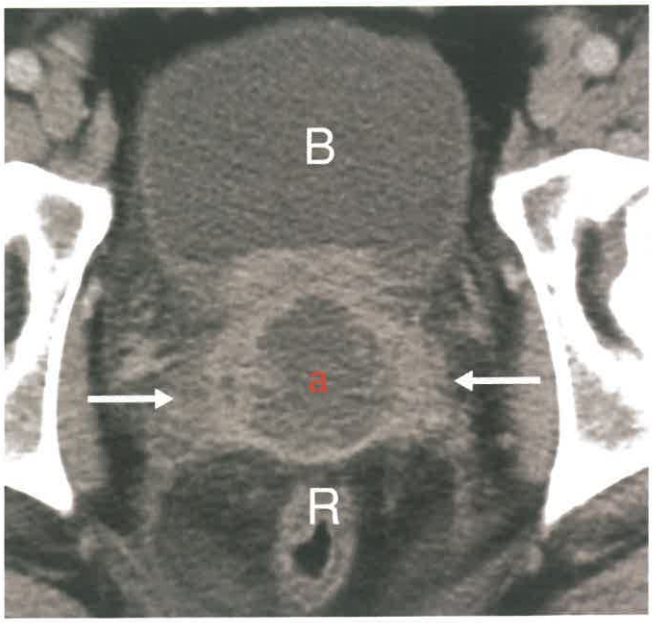

FIGURE 49.35. **Prostate Abscess.** Axial postcontrast CT shows a large irregular fluid collection (*a*) replacing and expanding most of the prostate gland representing an abscess. Periprostatic tissues (*arrows*) are infiltrated and edematous reflecting inflammation. *B*, bladder; *R*, rectum.

urethra obstructs bladder outflow and results in symptoms of hesitancy, decreased force and caliber of the urine stream, dribbling, frequency, nocturia, and postvoid residual. This progressive process is combated by hypertrophy of the bladder wall musculature (see Fig. 48.19). Advanced symptoms require medical therapy, balloon dilatation, stents, or transurethral resection of the prostate (TURP). CT findings of BPH include (a) enlargement of the prostate, commonly with lobulated contour and visible high and low attenuation nodules; (b) coarse calcifications (Fig. 49.34); (c) cystic degeneration; and (d) bladder wall thickening and trabeculation.

MR shows prostate enlargement with heterogeneous central gland on T2WI (Fig. 49.31). Areas of cystic degeneration are low signal on T1WI and high signal on T2WI. The stromal component of BPH can have low signal on T2WI mimicking cancer in the transitional zone. On diffusion-weighted ADC images, BPH shows restricted diffusion because of its highly cellular nature. On contrast-enhanced MRI, BPH shows increased abnormal perfusion.

Prostate abscess occurs as a common complication of bacterial prostatitis. Patients present with fever, dysuria, pelvic pain, and tenderness on transrectal prostate examination. Sepsis or failure to improve on antibiotic treatment suggests development of an abscess. US, CT, and MR show a complex fluid collection with prominent peripheral vascularity and inflammatory changes (Fig. 49.35).

Cystic lesions of the prostate and periprostatic tissues are uncommon but often prominent findings on prostate imaging. Congenital lesions include *Müllerian duct* and *prostatic utricle cysts* (Fig. 49.36) that occur in the midline in the upper half of the prostate. While these are separate entities they are indistinguishable by imaging. Small cysts are incidental findings. Larger cysts may cause bladder outlet obstruction symptoms, pain, and hematuria. CT shows a well-defined midline cyst of variable size. These cysts are high signal on T2WI. Prostate *retention cysts* result from obstruction of the prostatic ductule. They may occur anywhere in the gland and are usually small and asymptomatic. *Cysts associated with BPH* are the most common cysts of the prostate. Cystic appearance of *prostatic carcinoma* is rare but may be suspected if a cystic lesion shows rapid growth. *Abscesses* may complicated bacterial prostatitis and may be drained using TRUS guidance.

Seminal Vesicles

While primary tumors are rare, the seminal vesicles are commonly involved by tumors of the bladder, prostate, and rectum. Cysts and absence of the seminal vesicles are associated with ipsilateral renal dysgenesis or agenesis.

Anatomy. The seminal vesicles are paired elongated sac-like glands located in the posterior groove between the bladder base and the prostate. They produce 60% to 80% of the fluids passed during ejaculation. The dilated ampulla portion of the vas deferens courses just superior to the seminal vesicles. The vas deferens joins the ducts of the seminal vesicles to form the ejaculatory duct, which courses through the prostate gland

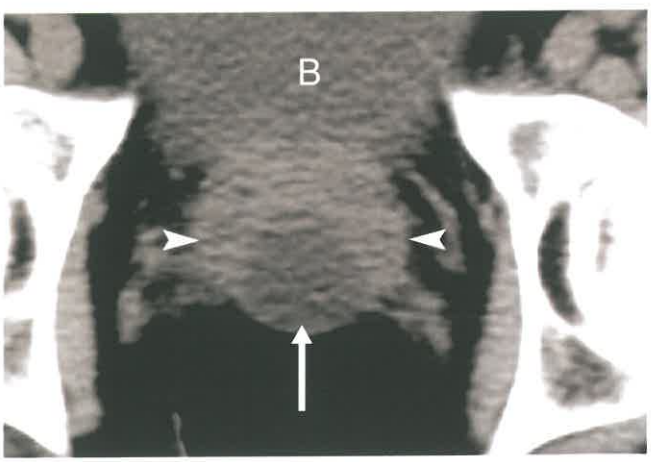

FIGURE 49.36. **Utricle/Müllerian Duct Cyst.** Axial CT without contrast shows a well-defined cyst (*arrow*) exactly in the midline of the prostate (between *arrowheads*). The patient was asymptomatic. This is an incidental finding of utricle cyst/Müllerian duct cyst. *B*, bladder.

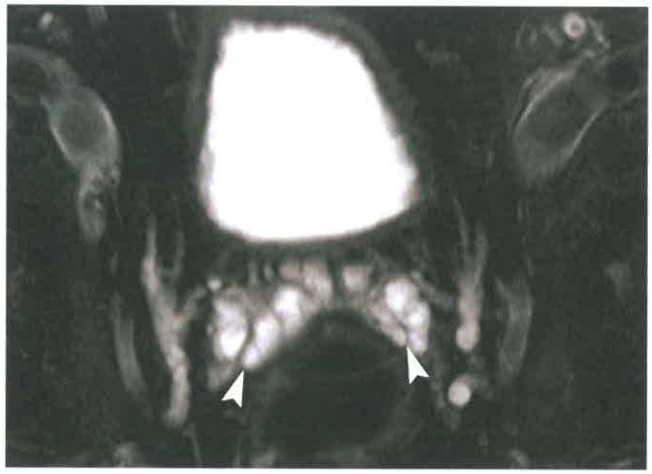

FIGURE 49.37. **Normal Seminal Vesicles.** T2-weighted axial plane MR with fat saturation shows the normal high signal intensity of the fluid-filled seminal vesicles (*arrowheads*).

to empty into the urethra at the level of the verumontanum. Normal seminal vesicles are 3 cm in length and 8 mm in diameter. Slight asymmetry is common. They contain fluid that is low to intermediate signal on T1WI and very high signal on T2WI (Fig. 49.37). The wall of the glands is 1 to 2 mm thick. The vas deferens is 3 to 5 mm in diameter. CT shows the fluid containing seminal vesicles as "bow-tie" in appearance on axial imaging. The seminal vesicles serve as a landmark for the lowest extent of the peritoneal cavity and for the location of the ureteral junctions with the bladder.

Pathology. Unilateral agenesis of the seminal vesicles is highly associated with ipsilateral renal agenesis (80% of cases). Bilateral seminal vesicle agenesis may be seen in some patients with cystic fibrosis. Hypoplasia occurs in association with cryptorchidism and hypogonadism. Cysts occur in patients with autosomal dominant polycystic disease and in association with developmental anomalies of the genitourinary tract. The extremely rare primary neoplasms include cystadenoma, cystadenocarcinoma, and sarcomas. Tumor involvement by prostate, bladder, or rectum carcinoma appears as contiguous solid tumor extending from the organ of origin to the seminal vesicles obliterating intervening fat planes. Bilateral calcification of the vas deferens is very highly associated with the presence of diabetes (Fig. 49.38).

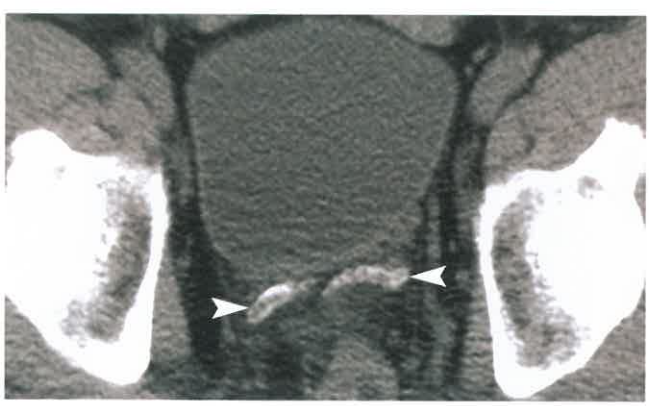

FIGURE 49.38. **Calcification of the Vas Deferens.** CT without contrast shows calcification of the bilateral vas deferens (*arrowheads*). This finding is almost universally associated with the presence of diabetes mellitus.

Penis

US and MR are the imaging modalities of choice for abnormalities of the penis. Indications include trauma, priapism, and tumors.

Anatomy. Both US and MR clearly delineate the anatomy of the penis (Fig. 49.27). The paired corpus cavernosa and the single corpus spongiosum containing the urethra are enveloped by the tough fibrous covering of the tunica albuginea. Buck fascia encases the corpora and deep vessels of the penis and fuses proximally with the deep urogenital fascia. A loose outer dartos facial layer is continuous with Colles fascia in the perineum. Hematomas or fluid collections within Buck fascia remain confined to the penis, while those external to Buck fascia may extend to the scrotum or anterior abdominal wall. Blood supply extends as branches of the internal pudendal artery, which arises from the internal iliac artery. Cavernosal arteries are imbedded within and supply the corpora cavernosa. Dorsal penile arteries and veins supply the glans penis, skin of the penis, and distal corpus spongiosum. The bulbar artery supplies the urethra and proximal corpus spongiosum.

Pathology. Penile fractures are uncommon and best evaluated initially by US, which demonstrates defects in the tunica albuginea and associated hematoma, usually confined within Buck fascia. On MR, the tunica albuginea is low signal and well demonstrated on both T1WI and T2WI. T1WI may detect subtle fractures obscured by high signal hematoma on T2WI. Diagnosis and surgical treatment are urgent as delay may result in erectile disorders and deformity. Painful penile induration, focal or generalized priapism, is most often caused by Peyronie disease, a connective tissue disorder, which produces plaques in the tunica albuginea resulting in penile curvature and deformity. Peyronie disease may present with acute pain or with chronic deformity. US and MR demonstrate focal fibrotic plaques causing thickening of the tunica albuginea. On MR, the plaques are low signal in concert with the tunica albuginea on both T1WI and T2WI. Contrast enhancement may be evident in the acute phase. Calcification may occur in the plaques in the chronic phase. Penile neoplasms are often accurately staged by clinical examination. MR is most accurate for imaging staging and for demonstrating adenopathy and tumor recurrence. Most tumors are squamous cell carcinomas or rare sarcomas. The cancers appear as an ill-defined infiltrating mass low in signal on both T1WI and T2WI. With intravenous contrast tumors enhance to a greater extent than the corpora.

Suggested Readings

Female Genital Tract

Agostinho L, Cruz R, Osíorio F, Alves J, Setúbal A, Guerra A. MRI for adenomyosis: a pictorial review. *Insights Imaging* 2017;8:549–556.

Allen BC, Hosseinzadeh K, Qasem SA, Varner A, Leyendecker JR. Practical approach to MRI of female pelvic masses. *AJR Am J Roentgenol* 2014;202:1366–1375.

Arleo EK, Schwartz PE, Hui P, McCarthy S. Review of leiomyoma variants. *AJR Am J Roentgenol* 2015;205:912–921.

Bérangeer-Gilbert S, Sakly H, Ballester M, et al. Diagnostic value of MR imaging in the diagnosis of adnexal torsion. *Radiology* 2016;279:461–470.

Coutinho A Jr, Bittencourt LK, Pires CE, et al. MR imaging in deep pelvic endometriosis: a pictorial essay. *Radiographics* 2011;31:549–567.

Javadi S, Ganeshan DM, Qayyum A, Iyer RB, Bhosale P. Ovarian cancer, the revised FIGO staging system, and the role of imaging. *AJR Am J Roentgenol* 2016;206:1351–1360.

Lalwani N, Prasad SR, Vikram R, Shanbhogue AK, Huettner PC, Fasih N. Histologic, molecular, and cytogenetic features of ovarian cancers: implications for diagnosis and treatment. *Radiographics* 2011;31:625–646.

Micco M, Sala E, Lakhman Y, Hricak H, Vargas HA. Imaging features of uncommon gynecologic cancers. *AJR Am J Roentgenol* 2015;205:1346–1359.

Moyle PL, Kataoka MY, Nakai A, Takahata A, Reinhold C, Sala E. Nonovarian cystic lesions of the pelvis. *Radiographics* 2010;30:921–938.

Olpin JD, Moeni A, Willmore RJ, Heilbrun ME. MR imaging of Müllerian fusion anomalies. *Magn Reson Imaging Clin N Am* 2017;25:563–675.
Revzin MV, Mathur M, Dave HB, Macer ML, Spektor M. Pelvic inflammatory disease: multimodality imaging approach with clinical-pathologic correlation. *Radiographics* 2016;36:1579–1796.
Sahin H, Abdullazade S, Sanci M. Mature cystic teratoma of the ovary: a cutting edge overview on imaging features. *Insights Imaging* 2017;8:227–241.
Simpson WL Jr, Beitia LG, Mester J. Hysterosalpingography: a reemerging study. *Radiographics* 2006;26:419–431.
Takeuchi M, Matsuzaki K. Adenomyosis: usual and unusual imaging manifestations, pitfalls, and problem-solving MR imaging techniques. *Radiographics* 2011;31:99–115.
Takeuchi M, Matsuzaki K, Nishitani H. Manifestations of the female reproductive organs on MR images: changes induced by various physiologic states. *Radiographics* 2010;30:1147–1148.

Male Genital Tract

Barentsz JO, Richenberg J, Clements R, et al. ESUR prostate MR guidelines 2012. *Eur Radiol* 2012;22:746–757.
Barrett T, Haider MA. The emerging role of MRI in prostate cancer active surveillance and ongoing challenges. *AJR Am J Roentgenol* 2017;208:131–139.
Boonsirikamchai P, Choi S, Frank SJ, et al. MR imaging of prostate cancer in radiation oncology: what radiologists need to know. *Radiographics* 2013;33:741–761.
Li Y, Mongan J, Behr SC, et al. Beyond prostate adenocarcinoma: expanding the differential diagnosis in prostate pathologic conditions. *Radiographics* 2016;36:1055–1075.
Mohrs OK, Thoms H, Egner T, et al. MRI of patients with suspected scrotal or testicular lesions: diagnostic value in daily practice. *AJR Am J Roentgenol* 2012;199:609–615.
Moreno CC, Small WC, Camacho JC, et al. Testicular tumors: what radiologists need to know—differential diagnosis, staging, and management. *Radiographics* 2015;35:400–415.
Parker RA 3rd, Menias CO, Quazi R, et al. MR imaging of the penis and scrotum. *Radiographics* 2015;35:1033–1050.
Purysko AS, Rosenkrantz AB, Barentsz, Weinreb JC, Macura KJ. PI-RADS version 2: a pictorial update. *Radiographics* 2016;36:1354–1372.
Rosenkrantz AB, Tenaja SS. Radiologist, be aware: ten pitfalls that confound the interpretation of multiparametric prostate MRI. *AJR Am J Roentgenol* 2014;202:109–120.
Vargas HA, Akin O, Franiel T, et al. Normal central zone of the prostate and central zone involvement by prostate cancer: clinical and MR imaging implications. *Radiology* 2012;262:894–902.